Available online at www.sciencedirect.com

ScienceDirect

Geochimica et Cosmochimica Acta 260 (2019) 329–348

Geochimica et Cosmochimica Acta

www.elsevier.com/locate/gca

Isotopic records of climate seasonality in equid teeth

Scott A. Blumenthal [a,*], Thure E. Cerling [b], Tara M. Smiley [c], Catherine E. Badgley [d], Thomas W. Plummer [e,f,g]

[a] Department of Anthropology, University of Oregon, Eugene, OR, USA
[b] Department of Geology & Geophysics, University of Utah, Salt Lake City, UT, USA
[c] Environmental Resilience Institute, Indiana University, Bloomington, ID, USA
[d] Department of Ecology & Evolutionary Biology, University of Michigan, USA
[e] Department of Anthropology, Queens College, Flushing, NY, USA
[f] Department of Anthropology, The Graduate Center, New York, NY, USA
[g] New York Consortium in Evolutionary Primatology, New York, NY, USA

Received 24 May 2017; accepted in revised form 23 June 2019; available online 2 July 2019

Abstract

We investigate how oxygen isotopes in equid teeth can be used as a record of seasonality. First, we use *in situ* laser ablation and conventional microsampling techniques to understand time-averaging of environmental signals in intra-tooth isotope profiles in modern feral horse teeth (n = 5) from Mongolia, where there is a large seasonal gradient in the oxygen isotopic composition of precipitation. We demonstrate that laser ablation can be used to sample inner, middle, and outer enamel layers in large mammalian herbivore teeth. The inner enamel layer records less attenuated isotopic signals than other layers, as predicted by the mineralization patterns, but intra-tooth signal amplitude is similar for laser and conventional sampling methods. Second, we use modern zebra teeth (n = 21) collected in eastern Africa to evaluate how intra-tooth oxygen isotope variation relates to rainfall patterns in the tropics. We show that the intra-tooth isotopic range increases with intra-annual precipitation isotopic range, which in turn relates to aridity in the equatorial bimodal rainfall region but is influenced by other hydroclimate processes in the region as a whole. Finally, we address isotopic seasonality during the Early Pleistocene in eastern Africa using oxygen isotopes in fossil equid teeth from southwestern Kenya (n = 11) and northern Tanzania (n = 5). We find variable isotopic seasonality in the past, similar to present-day eastern Africa, consistent with the notion that hominins and other mammals were able to accommodate environmental variability on intra-annual scales in addition to well-documented orbital cycles.

Keywords: Tooth enamel; stable isotopes; microsampling; seasonality; eastern Africa

1. INTRODUCTION

In the tropics today, climate seasonality (intra-annual precipitation cycles) is a primary determinant of vegetation structure (Good and Caylor, 2011; Staver et al., 2011; Guan et al., 2014), fire regime (Lehmann et al., 2014; Archibald and Hempson, 2016), primary productivity (Guan et al., 2013, 2015), biogeochemical cycling (Knapp et al., 2008; Feng et al., 2012; Rohr et al., 2013; Runyan and D'Odorico, 2013), and mammal population dynamics (Ogutu and Owen-Smith, 2003). Rainfall seasonality may be important for understanding past ecosystem change, such as the expansion of C_4 plants since the late Miocene (Osborne, 2008; Strömberg, 2011; Karp et al., 2018) as well as changes in the environments of early hominins and other

* Corresponding author.
E-mail address: sblument@uoregon.edu (S.A. Blumenthal).

https://doi.org/10.1016/j.gca.2019.06.037
0016-7037/

mammals in Africa (Foley, 1993; Kingston, 2005; Levin, 2015). A number of approaches have been developed to assess aspects of climate seasonality in the fossil record, including (1) paleolimnological proxies such as diatoms, pollen, or leaf wax biomarkers (Stager et al., 2003; Vincens et al., 2007; Verschuren et al., 2009; Barker et al., 2011; Wilson et al., 2014); (2) paleosol carbonate horizon thickness (Retallack, 2005); (3) isotopic microsampling of invertebrate shells (Hailemichael et al., 2002; Vonhof et al., 2013); (4) periodicity of stress lines in mammal teeth (Macho et al., 2003); (5) cementum accretion analysis (Wall-Scheffler and Foley, 2008; Lam, 2008); (6) dental wear patterns (Sánchez-Hernández et al., 2016); and (7) plant macrofossil morphology (Jacobs and Schloeder, 2002; Peppe et al., 2011; Bamford et al., 2013). In addition, intra-tooth isotopic variation in mammal teeth offers a promising alternative for addressing seasonal-scale changes in behavior or environmental conditions terrestrial.

Stable isotope analysis of animal bones and teeth is a well established method in archaeological, paleontological, and geological research for diet and climate studies (Kohn and Cerling, 2002; Lee-Thorp, 2008; Clementz, 2012). Isotopic variation on seasonal scales, within the lifetimes of individual animals, can be recovered by sampling tissues that grow incrementally and do not remodel after formation, such as teeth. Tooth dentine provides high resolution intra-tooth isotopic records (Zazzo et al., 2006; Codron et al., 2012), but tooth enamel is preferred in fossil studies because it is more resistant to diagenetic alteration (Wang and Cerling, 1994; Lee-Thorp and Sponheimer, 2003). Intra-tooth isotopic records are chronologically ordered, spanning the period of enamel formation and maturation, and preserve behavioral or environmental information on intra-annual time scales (Kohn et al., 1998; Balasse, 2002; Passey and Cerling, 2002; Zazzo et al., 2010; Green et al., 2018b). Stable isotope ratios of oxygen measured in tooth enamel ($\delta^{18}O_{enamel}$) reflect body water, which is a function of the oxygen isotopic composition of inspired air and meteoric (precipitation-derived) water ($\delta^{18}O_{mw}$) ingested directly by drinking and indirectly in food (Bryant and Froelich, 1995; Kohn, 1996; Podlesak et al., 2008; Green et al., 2018a). Variation in the oxygen isotopic composition of precipitation ($\delta^{18}O_{precip}$) relates primarily to temperature and rainfall amount (amount effect) in high and low latitudes, respectively (Dansgaard, 1964; Rozanski et al., 1993; Bowen and Revenaugh, 2003), including seasonal (intra-annual) $\delta^{18}O_{precip}$ variation (isotopic seasonality) (Bowen, 2008). Oxygen isotope ratios of surface and plant waters can be further modified by evaporation and transpiration, such that $\delta^{18}O$ values of standing water sources (e.g. lakes) and leaf water can be higher than $\delta^{18}O$ values of meteoric water (Jasechko et al., 2013; Cernusak et al., 2016). Thus, the degree of water-dependence of animals is critical for understanding how enamel $\delta^{18}O$ relates to meteoric water (Kohn et al., 1996; Levin et al., 2006; Blumenthal et al., 2017). Following from these principles, intra-tooth oxygen isotope records have been used to address past climate seasonality (Sharp and Cerling, 1998; Higgins and MacFadden, 2004; Nelson, 2005; Bernard et al., 2009; Souron et al., 2012; Metcalfe and Longstaffe, 2014; D'Ambrosia et al., 2014; Zanazzi et al., 2015; Hartman et al., 2016; Reade et al., 2018).

Equid check teeth (premolars and molars) are ideal candidates for reconstructing seasonality because these highly hypsodont teeth grow over 2–3 years, potentially preserving multiple seasonal cycles (Hoppe et al., 2004). Modern equids are water-dependent grazers (Western, 1975; Crowell-Davis et al., 1985; Scheibe et al., 1998; Bahloul et al., 2001; de Leeuw et al., 2001; King, 2002; Redfern et al., 2003; Sitters et al., 2009; Ogutu et al., 2010), and among analyzed feral and wild equids tooth $\delta^{18}O_{enamel}$ reflects meteoric water, the primary drinking water source (Bryant et al., 1994; Huertas et al., 1995; Sharp and Cerling, 1998; Hoppe et al., 2005; Levin et al., 2006; Blumenthal et al., 2017). Seasonal-scale isotopic variation in equid teeth has been documented by previous studies on modern, archaeological, and paleontological specimens from Africa (Kohn et al., 1998; di Lernia et al., 2013; Lüdecke et al., 2016; Uno et al., 2018), North America (Sharp and Cerling, 1998; Kohn et al., 2002; Higgins and MacFadden, 2004; MacFadden, 2008; Feranec et al., 2009), Asia (Nelson, 2005; Wang et al., 2008; Zhang et al., 2009, 2012; Bendrey et al., 2015), Europe (Pellegrini et al., 2008; van Dam and Reichart, 2009; Fabre et al., 2011; Rivals et al., 2014; Julien et al., 2015; de Winter et al., 2016), and the Middle East (Wiedemann et al., 1999; Bocherens et al., 2001). However, despite the relative abundance of equid intra-tooth isotope records, and extensive studies on enamel maturation and microsampling in mammals generally (Passey and Cerling, 2002; Zazzo et al., 2005; Blumenthal et al., 2014; Trayler and Kohn, 2017; Green et al., 2018b), there remains no straightforward model to quantitatively infer aspects of climate from intra-tooth profiles of equids or other mammals. Significantly, the relationship between intra-annual isotopic variation of precipitation and intra-tooth isotopic variation of enamel, and how either of these parameters relate to intra-annual climatic variation, remains poorly understood.

The climate in eastern Africa is complex, driven by atmospheric circulation and topography, and the intra-annual distribution of rain varies across the region (Nicholson, 2017). Most of eastern Africa is characterized by bimodal rainfall (boreal spring and autumn), termed the "equatorial rainfall region" (Nicholson, 2017). The bimodal rainfall pattern has traditionally been explained by the seasonal passage of the Intertropical Convergence Zone (ITCZ) (Ogallo, 1989; Nicholson, 1996, 2000); however, recent meteorological studies demonstrate that regions of wind convergence associated with the ITCZ do not correspond with areas of rainfall, and show that low-level atmospheric winds are divergent over most of the region during the rainy seasons (Yang et al., 2015; Nicholson, 2018). Instead, rainfall is associated with seasonal variation in atmospheric convective stability (surface moist static energy and vertically integrated moisture flux) and sea surface temperatures in the western Indian Ocean (Yang et al., 2015). Precipitation during both rainy seasons, mostly falling during daytime, is brought by warm, moist air flowing from the southwestern Indian Ocean (southeast-

erlies). During boreal winter and summer, rainfall is suppressed by the flow of air from the cool Indian Ocean and by the low-level Turkana Jet (Yang et al., 2015; Nicholson, 2016). Areas deviating from the equatorial rainfall regime include: (1) the boreal summer rainfall sector, including much of Ethiopia, northern Uganda, and South Sudan, which is influenced by the West African monsoon and where moisture is transported from the Indian Ocean, Atlantic Ocean, and Mediterranean (Levin et al., 2009; Viste and Sorteberg, 2013); (2) the narrow strip along the eastern African coast, where boreal summer rainfall is controlled by sea breeze circulation and its interaction with Indian Ocean monsoons (Camberlin and Planchon, 1997); (3) areas within and immediately adjacent to Lake Victoria, influenced by mesoscale moisture circulation and lake surface temperature (Yin et al., 2000; Sun et al., 2015); (4) areas of high relief, relating to orographic uplift and local winds (Oettli and Camberlin, 2005; Hession and Moore, 2011; Camberlin et al., 2014); (5) nonseasonal humid regime within a narrow equatorial band extending east from the Congo Basin to western Kenya (Nicholson, 2000; Herrmann and Mohr, 2011). Such variability in rainfall patterns across eastern Africa, associated with changes in circulation patterns and moisture source, likely accounts for previous studies finding no relationship between seasonal precipitation $\delta^{18}O$ values and rainfall amount (Bowen, 2008), or between meteoric water $\delta^{18}O$ values and aridity (Blumenthal et al., 2017). Thus, although $\delta^{18}O_{precip}$ values do vary seasonally in eastern Africa (Rozanski et al., 1996; Bowen, 2008), the relationship between isotopic variability and climate is complicated (Konecky et al., 2019).

In this study, we address the problem of reconstructing climate seasonality using intra-tooth isotopic records from equid teeth. First, we test alternative sampling strategies in modern horse teeth by comparing *in situ* laser ablation analysis of bulk enamel with conventional acid digestion analysis of the carbonate component of hand drilled enamel. We use horse (*Equus ferus przewalskii*) teeth from Mongolia, where there is strong intra-annual variability in $\delta^{18}O_{precip}$ and herbivore $\delta^{18}O_{enamel}$ (Stacy, 2008; Makarewicz and Pederzani, 2017), to test the effectiveness of sampling inner enamel for recovering greater amplitude ($\delta^{18}O_{enamel}$ range) in intra-tooth profiles. Second, we evaluate the relationship between intra-tooth $\delta^{18}O_{enamel}$ variability and intra-annual $\delta^{18}O_{precip}$ variability using plains zebra (*Equus quagga*) teeth from eastern Africa. Third, we address the climatological significance of intra-annual $\delta^{18}O_{precip}$ variability in eastern Africa in order to understand which aspects of climate can be inferred from intra-tooth $\delta^{18}O_{enamel}$ records. Finally, we use intra-tooth $\delta^{18}O_{enamel}$ variability from Pleistocene equids, including specimens from archaeological sites in southwestern Kenya and northern Tanzania, to infer past isotopic seasonality in hominin environments based on relationships between intra-tooth $\delta^{18}O_{enamel}$ and intra-annual $\delta^{18}O_{precip}$ variability among modern zebra. We focus on the Early Pleistocene, an important period of human evolution associated with significant changes in encephalization, diet, technology, and mobility (Antón et al., 2014).

2. TOOTH ENAMEL

Tooth enamel is a calcium phosphate $Ca_{10}(PO_4)_6(OH)_2$ with structural carbonate (CO_3) present as a substitute for phosphate (PO_4) in the β position (~90%) and as a substitute for hydroxyl (OH) in the α position (~10%) (LeGeros et al., 1969; Elliott et al., 1985; Elliott, 2002). Oxygen in tooth enamel is present in the phosphate, carbonate, and hydroxyl groups, with oxygen contents of 35%, 3.3%, and 1.6%, respectively (Cerling and Sharp, 1996). Each component is in isotopic equilibrium with body water and with each other. The oxygen isotope fractionation between phosphate (low) and carbonate (high) is typically ca. 9‰, varying from ~6‰ to ~12‰ (Bryant et al., 1996; Iacumin et al., 1996; Martin et al., 2008; Pellegrini et al., 2011). The fractionation between phosphate and hydroxyl has been indirectly estimated as −16.6‰ (Jones et al., 1999). Analyzing targeting different components of enamel is expected to provide different oxygen isotope values, with *in situ* analysis reflecting bulk enamel, which is mostly phosphate assuming complete mixing.

Enamel formation is a multi-stage process, including the appositional (or secretary) stage and the maturation stage (Robinson et al., 1978; Suga, 1982; Robinson et al., 1995; Moss-Salentijn et al., 1997; Beniash et al., 2009; Simmer et al., 2012). During apposition, an organic-rich matrix is secreted in layers at a low angle to the enamel-dentine junction (EDJ). Successive positions of appositional growth are visible in mature enamel as incremental growth features (Hoppe, 2004; Tafforeau et al., 2007; Kierdorf et al., 2013). The mineral content of appositional enamel increases to ~15–25% by weight, except within the more highly mineralized innermost enamel layer ~10–20 μm from the EDJ (Suga, 1982; Tafforeau et al., 2007; Blumenthal et al., 2014). During maturation, the removal of matrix proteins and fluid content is accompanied by crystal growth and increasing calcium and phosphate ion uptake, such that mineral content increases to ~95–98% by weight in mature enamel (Hiller et al., 1975; Robinson et al., 1979; Suga, 1982; Robinson et al., 1997; Smith, 1998; Passey and Cerling, 2002). Maturation appears to follow a complex geometry, variably described as following (1) a low angle to the EDJ, similar to appositional growth (Passey and Cerling, 2002; Hoppe et al., 2004; Zazzo et al., 2005), (2) a high angle to the EDJ, roughly perpendicular to the outer enamel surface (Trayler and Kohn, 2017), and (3) a spatially diffuse wave with no discernible maturation front (Tafforeau et al., 2007; Green et al., 2017). These models of enamel mineralization are based on observations made using radiographic images, spectrophotometry, X-ray imaging, and scanning electron microscopy, which may capture different aspects of mineral density, and the degree to which maturational differences reflect biological or methodological variation deserves further study. Previous studies have consistently documented that inner and middle enamel layers (~75% of thickness) mineralize earlier than outer enamel (~25%) (Suga, 1982; Blumenthal et al., 2014; Trayler and Kohn, 2017). Carbonate content declines during maturation on both a mineral-weight basis (ca. 2–5% in mature enamel) and relative to phosphate content

(Hiller et al., 1975; Aoba and Moreno, 1990; Sydney-Zax et al., 1991; de Winter et al., 2016). The final mineral content of inner enamel is lower than outer enamel (Suga, 1983), and higher carbonate content near the EDJ compared to near the outer enamel surface may reflect greater retention of earlier forming enamel mineral (Weatherell et al., 1968; Hiller et al., 1975; Zazzo et al., 2005).

3. INTRA-TOOTH ISOTOPIC SIGNALS AND SAMPLING

Conventionally, intra-tooth samples are collected by drilling several mm^3 of enamel in horizontal grooves perpendicular to the growth axis and extending from the outer surface partially or entirely through the thickness of enamel (Balasse, 2002). Idiosyncratic variation in the volume and location of individual grooves, unavoidable when hand-drilling, is likely unimportant as intra-tooth isotopic profiles are to a large extent insensitive to differences in sampling strategy (Passey and Cerling, 2002; Green et al., 2018b). Small differences in enamel thickness incorporated into individual samples could contribute to signal blurring if outer and middle enamel reflect different maturation time intervals, but this is likely a minor effect particularly in taxa where enamel maturation follows a high angle to the EDJ, such as equids (Trayler and Kohn, 2017). Additionally, each intra-tooth sample, regardless of how small, integrates isotopic input spanning the length of maturation and does not represent instantaneous or even discrete intervals of time (Passey and Cerling, 2002; Hoppe et al., 2004; Zazzo et al., 2005; Blumenthal et al., 2014). The maturation length varies among taxa, although in some cases maturation appears non-linear with rapid mineralization occurring over a relatively short distance, and possibly isotopically resets appositional enamel (Trayler and Kohn, 2017; Green et al., 2018b). Among common mammalian herbivores intra-tooth samples appear to correspond to intervals of weeks to months (Kohn, 2004; Hoppe et al., 2004; Trayler and Kohn, 2017; Green et al., 2018b). Consequently, intra-tooth isotopic signals are time-averaged relative to primary isotopic time-series of the body pool and relative to temporal variation in diet or environmental conditions, well-documented in diet- and water-switch experiments (Balasse, 2002; Zazzo et al., 2005; Passey et al., 2005; Podlesak et al., 2008; Zazzo et al., 2010; Green et al., 2018b). Signal damping can alter both signal amplitude and structure, with severity dependent on maturation length and primary signal duration and structure (Kohn, 2004; Passey and Cerling, 2004; Passey et al., 2005; Green et al., 2018b).

Intra-tooth sampling strategies should be guided by the geometry of maturation, which determines the distribution of isotopes in enamel (Balasse, 2003; Blumenthal et al., 2014; Trayler and Kohn, 2017). Sampling parallel to incremental features may minimize the integration of appositional growth increments, but is not effective at reducing signal blurring even when maturation mimics the geometry of apposition (extending from the EDJ at a similarly low angle) (Zazzo et al., 2005), and may worsen signal blurring in cases where maturation proceeds at a high angle to the EDJ (Trayler and Kohn, 2017). A more effective strategy is to target enamel zones that mineralize more rapidly (Balasse, 2003; Zazzo et al., 2005; Tafforeau et al., 2007; Metcalfe and Longstaffe, 2012; Zazzo et al., 2012; Blumenthal et al., 2014; Trayler and Kohn, 2017). The innermost enamel layer, extending <20 μm from the enamel-dentine junction, mineralizes most rapidly and appears to retain significantly less altered intra-tooth isotopic signals (Tafforeau et al., 2007; Blumenthal et al., 2014). The innermost enamel layer can be sampled using secondary ion mass spectrometry (SIMS), a powerful tool for resolving isotopic differences on a fine spatial scale (Blumenthal et al., 2014), although this approach has not been widely applied due to cost, limited availability of instrumentation, specimen size, and specimen preparation limitations. A more accessible strategy may be to target inner enamel, rather than specifically the innermost layer, which nonetheless mineralizes more rapidly than outer enamel, appears to retain less blurred intra-tooth signals, and can be analysed using more widely available instrumentation, such as laser ablation, micromilling, or tooth dicing (Zazzo et al., 2005; Metcalfe and Longstaffe, 2012; Blumenthal et al., 2014; Trayler and Kohn, 2017; Green et al., 2018b). This approach requires teeth where inner enamel is exposed by sectioning or by natural damage.

In this study, we test the effectiveness of inner enamel sampling in horse teeth using laser ablation, a microsampling method with sufficient spatial resolution (ca. 100–200 μm) to target discrete enamel zones (excluding the innermost layer) (Passey and Cerling, 2006). *In situ* analysis of bulk enamel mixes multiple oxygen-bearing components, but is dominated by phosphate (~90%) with minor contributions by carbonate (~6%) and hydroxyl (~3%) groups. We compare laser profiles (bulk enamel) to conventional hand drilled sequential samples of (enamel carbonate), following previous studies applying laser ablation methods to tooth enamel (Cerling and Sharp, 1996; Passey and Cerling, 2006; Sponheimer et al., 2006; Lee-Thorp et al., 2012; Garcia et al., 2015). Although carbonate represents a smaller fraction of oxygen in enamel compared to phosphate, the isotopic composition of bulk enamel and carbonate have a 1:1 relationship (Passey and Cerling, 2006). Carbon isotopic enrichment between carbonate and bulk enamel is -0.3 ± 1.1‰ for modern enamel and -0.5 ± 0.8‰ for fossil enamel, and oxygen isotopic enrichment between carbonate and bulk enamel is -6.4 ± 0.7‰ for modern enamel and -5.1 ± 1.2‰ for fossil enamel (Passey and Cerling, 2006). The timing and routing of mineral uptake and oxygen isotope incorporation in carbonate versus phosphate components may vary, but evidence that this impacts intra-tooth signal fidelity is equivocal (Pellegrini et al., 2011; Trayler and Kohn, 2017).

Mathematical models provide another way to interpret intra-tooth isotope profiles. Inversion methods provide a potentially powerful means to estimate primary input signal amplitude and structure, based on sampling and mineralization geometry (Passey et al., 2005; Green et al., 2018b). The (Passey et al., 2005) model works well when applied to continuously growing teeth with roughly constant growth rates, such as hippopotamus canines (Cerling

et al., 2008) or rodent incisors (Podlesak et al., 2008; Blumenthal et al., 2014). However, we do not apply the model here because teeth of equids and other large mammal teeth violate model assumptions, including continuous and linear growth (Zazzo et al., 2012; Bendrey et al., 2015; Nacarino-Meneses et al., 2017) and alignment of maturation geometry with incremental growth features (Tafforeau et al., 2007). Additionally, inversion estimates from this model are sensitive to small isotopic changes such that high analytical reproducibility (<0.1‰) is needed to produce interpretable results (Passey et al., 2005). A recently developed alternative model (Green et al., 2018b) addresses some of these problems, particularly nonlinear tooth growth as well as spatial and temporal complexity of enamel mineralization, and can accurately recover the structure and timing of water input signals from oxygen isotope profiles from enamel phosphate of sheep molars. Applying the model to other mammals (such as equids) and to measurements of enamel carbonate rather than phosphate may require additional model development and/or validation, which lies beyond the scope of this study, and we do not discuss this model further.

We focus on estimating only the amplitude of environmental signals from intra-tooth isotope profiles, which can be addressed in a more straightforward manner. Following (Kohn, 2004), damping (d), of signal amplitude can be calculated by comparing the amplitude of the environmental signal (a_e) with the recorded signal (a_r):

$$d = \frac{a_e - a_r}{a_e} \quad (1)$$

where a_e is the intra-annual range of $\delta^{18}O_{precip}$ values and a_r is the intra-tooth range of $\delta^{18}O_{enamel}$ values. The damping factor ranges from 0 (perfect signal) to 1.0 (all signal lost). Signal amplitudes in fossil teeth can be corrected using the damping factor calculated using specimens of modern representatives. The corrected (undamped) intra-tooth range of $\delta^{18}O_{enamel}$ values can be calculated using the following equation:

$$a_c = \frac{a_r}{1 - d} \quad (2)$$

where a_c is the corrected (undamped) $\delta^{18}O_{enamel}$ intra-tooth range. We use this approach to address the relationship between the intra-tooth range in $\delta^{18}O_{enamel}$ values and the intra-annual range in $\delta^{18}O_{precip}$.

4. MATERIALS AND METHODS

4.1. Extant specimens

Mature teeth (n = 5) from feral horses were collected from naturally deceased free-range individuals in northern Mongolia for isotopic analysis, and additionally a tooth germ (n = 1) was used for enamel maturation analysis. Rainfall and temperature in this region are highly seasonal, with one long summer rainy season (Cerling and Harris, 1999). Precipitation oxygen isotope measurements from Ulaanbaatar, Mongolia are used for comparison (Aggarwal et al., 2008). Zebra teeth were collected in maxillary bone from naturally deceased wild zebra in Kenya, including Amboseli (n = 8), Laikipia (n = 3), and Turkana (n = 2), and Uganda, including Lake Mburo National Park (n = 5), Kidepo (n = 3). Additional information on modern teeth (element, collection date) is available in Table A.1. Age of death is unknown, but likely ranges from a few years to a decade prior to collection date, based on taphonomic studies of skeletal preservation in African ecosystems (Behrensmeyer, 1978; Tappen, 1994).

Annual and monthly average isotopic values were obtained from a regionalized cluster-based water isotope prediction (RCWIP) model based on the International Atomic Energy Agency (IAEA) Global Network of Isotopes in Precipitation (GNIP) (Terzer et al., 2013). We compare $\delta^{18}O_{precip}$ values to climate variables based on data (~1 km^2 resolution) from WorldClim 2 (Fick and Hijmans, 2017), including mean annual precipitation, precipitation seasonality, and water deficit for a set of eastern African sites used in previous analyses of isotope-climate relationships (Table A.2) (Blumenthal et al., 2017). We calculate water deficit following (Thornthwaite, 1948) using monthly temperatures from WorldClim 2, which differs from previous water deficit calculations for these sites using mean annual temperatures from weather observation data (Levin et al., 2006; Blumenthal et al., 2017).

4.2. Fossil specimens

Fossils sampled for this study were collected from Pleistocene sediments on the Homa Peninsula, southwestern Kenya. Nine specimens are derived from the Kanjera Formation, a 36 m thick sequence exposed north of the Homa Mountain complex and divided into two members (South and North) (Ditchfield et al., 1999). The Kanjera South Member includes Early Pleistocene sediments exposed at the Kanjera South locality and is comprised of five beds, from oldest to youngest KS1 to KS5. Equid cheek teeth were selected from KS1 (n = 3) and KS2 (n = 5), which contain abundant *in situ* fossil and Oldowan archaeological materials in fluvio-lacustrine sediments dated to ~2.0 Ma based on a combination of biostratigraphy and magnetostratigraphy (Ditchfield et al., 1999; Plummer et al., 2009b; Ditchfield et al., 2018). The Kanjera North Member includes Early to Middle Pleistocene sediments exposed at the Kanjera North locality and is comprised of 5 beds, from oldest to youngest KN1 to KN5. One equid cheek tooth was selected from KN3, a bed that includes both *in situ* and surface collections of mammalian fossils and Early Stone Age artifacts (Plummer, 1991; Behrensmeyer et al., 1995; Ditchfield et al., 1999). The Kasibos Formation, exposed at Kanam East, is ca. 7 m thick clay-dominated sequence dated to ~1.0 Ma based on a combination of biostratigraphy and magnetostratigraphy (Ditchfield et al., 1999). A diverse large mammal fauna has been collected on the surface and *in situ* and collected surface artifacts include Acheulean bifaces and other lithics that may be derived from the Kasibos Formation, or associated with the poorly defined Abundu Formation (Ditchfield et al., 1999).

We also include previously published fossil equid data from sites in northern Tanzania. Sites at Olduvai Gorge

famously preserve dense concentrations of Early Stone Age artifacts and mammal fossils, and we include teeth (n = 3) from Olduvai Gorge Bed II sites MNK Main, FC West, HWK EE sites (Uno et al., 2018). The HWK EE trench is stratigraphically positioned between Tuffs IIA and Tuff IIB, and dates to ~1.7 Ma based on estimated age of Tuff IIA (McHenry and Stanistreet, 2018), while NMK Main and FC West trenches are positioned between Tuffs IIB and IIC in close proximity to the Bird Print Tuff (BPT) dated to 1.664 ± 0.019 Ma (Diez-Martín et al., 2015). We also include teeth (n = 2) from the MK4 locality in the upper part of the lower member of the Manyara Beds, exposed in the Makuyuni area and rich in mammal fossils and Early Stone Age artifacts, dating to between 0.784 and 0.633 Ma based on magnetostratigraphy and the MK16P $^{40}Ar/^{39}Ar$ age (Wolf et al., 2010; Schwartz et al., 2012).

4.3. Enamel mineralization analysis

As previously reported (Blumenthal et al., 2014), a Mongolian horse tooth germ was embedded in epoxy and imaged uncoated in variable pressure mode (50 Pa) using a Zeiss EVO-50 (Thornwood, New York) scanning electron microscope in backscattered electron imaging mode at 15 kV, 600 pA, and 8.5-mm working distance (Fig. A.1). Two mineral density standards were used, including 99% aluminum with a mineral density similar to mature enamel and an iodinated methacrylate standard ($C_{22}H_{25}O_{10}I$) with a mineral density between dentine and enamel (Boyde et al., 1995). Image montages were acquired automatically using Zeiss SmartStich software, and ImageJ (NIH) was used to measure image intensity (gray level) of individual pixels. Gray levels relate to the number of measured backscattered electrons, which is a function of mean atomic number of the material and to weight percent mineral (Bloebaum et al., 1997). Gray levels range from 0 for black (no mineral) and 255 for white (most mineral). As previously reported, gray levels of 222 (Al standard) correspond with 99% mineral, and gray level of 0 (epoxy) represents 0% mineral. Mature enamel for this specimen has a mean gray level of 221 and mature dentine has a mean gray level of 132, corresponding to 98% and 59% mineralization. Gray level transects presented previously from the same equid tooth germ (Blumenthal et al., 2014) targeted the very thin innermost and outermost (or 'subsurface') enamel layers (<20 μm), corresponding to zones of particularly fast and slow mineralization, with remaining enamel was divided arbitrarily into layers of equal thickness. In this study, the innermost or outermost enamel layers are not relevant, as we do not target this zone for isotope analysis. We assess enamel maturation at the spatial scale relevant to laser ablation, and re-measure gray levels using 100 μm-thick transects parallel to the growth axis through inner, middle, and outer thirds of the enamel layer, following previous mineralization studies showing variable mineralization patterns within the thickness of the enamel layer (Suga, 1982, 1983; Blumenthal et al., 2014; Trayler and Kohn, 2017). The division of the enamel layer into 3 zones of equal thickness can be readily extended to other taxa, regardless of variation in enamel thickness, microstructure, or mineralization patterns. In this study, gray level transects are measured from the beginning of the maturation stage, excluding the innermost enamel layer. This position is ca. 8 mm from the position at which the mineral contents of the innermost enamel layer begins to increase (Blumenthal et al., 2014).

4.4. *In situ* isotope analysis using laser ablation (LA-GC-IRMS)

Columns of anterior or central buccal enamel from Mongolian horse teeth were cut into thick sections for laser ablation analysis using a Buehler Isomet (Evanston, IL) with a diamond wafering blade and 70% ethanol solution. Tooth sections were placed in the sample chamber and purged with He overnight prior to each analytical session. *In situ* laser ablation sampling was performed at the University of Utah using a CO_2 laser (6.6–7.5 W, 8.5 ms pulse duration, 10.6 μm wavelength), operating in a helium purged positive pressure environment, that thermally ablates enamel in pits several hundred μm in diameter and ~100 μm in depth (Passey and Cerling, 2006). CO_2 generated from 3-6 ablation events was cryogenically concentrated prior to inlet to a gas chromatograph (flow rate = 250 ml/min, GC temperature = 60 °C), and analyzed on a Finnigan MAT 252 isotope ratio mass spectrometer (IRMS) in continuous flow mode via a GP interface. Internal laboratory CO_2 gas and tooth enamel standards were analyzed to monitor systematic and laser ablation fractionation, respectively, using the same standards as previous laser ablation studies (Kimura et al., 2013). Spots were placed parallel to the growth axis within the inner, middle, and outer thirds of the enamel thickness (Fig. A.2). After isotopic analysis teeth were examined under optical light microscope, and laser spots with visible charring of organic material or overlapping with cracks or edges were removed from subsequent analyses. Analytical precision was <0.8‰ for $\delta^{13}C$ and $\delta^{18}O$, which is typical for laser ablation (Passey and Cerling, 2006).

4.5. Conventional isotope analysis

Tooth enamel to be analyzed conventionally by acid digestion of enamel carbonate was sampled using a handheld rotary drill with a diamond bit (Fig. A.3). Cementum or matrix was first removed, if needed, and the enamel surface was cleaned with ethanol before sampling. Enamel powder was collected along the growth axis from ca. 1 mm wide grooves at ca. 3–5 mm intervals, taking great care to avoid the underlying dentine. Enamel was chemically treated before isotopic analysis using standard procedures to remove organic contaminants (3% H_2O_2) in modern teeth and secondary exogenous carbonates (0.1 M buffered acetic acid) in fossil teeth (Koch et al., 1997; Sponheimer and Cerling, 2014). At the University of Utah, enamel powder samples were reacted with >100% H_3PO_4 at 90 °C in silver capsules using a Finnigan CarboFlo, which is a hybrid positive pressure/vacuum system with a common acid bath. $^{13}C/^{12}C$ and $^{18}O/^{16}O$ ratios of enamel carbonate were measured by analyzing the resulting CO_2

with a dual inlet isotope ratio mass spectrometer (Finnigan MAT 252). Data were corrected with Carrara carbonate and internal laboratory fossil enamel standards. Analytical precision was <0.2‰ for $\delta^{13}C$ and $\delta^{18}O$ for modern and fossil teeth. All isotopic ratios are reported using conventional per mil (‰) notation where $\delta^{18}O_{sample} = (R_{sample}/R_{standard} - 1) \times 1000$. Numerous studies have demonstrated that tooth enamel is resistant to diagenetic alteration over geologic time, and there are no clear relationships between mineralogical, crystallographic, and chemical changes in enamel with isotopic alteration (Wang and Cerling, 1994; Zazzo et al., 2004; Lee-Thorp, 2008; Roche et al., 2010). Diagenesis was monitored by CO_2 yield, since the addition of pure (100%) inorganic carbonates will markedly increase the amount of CO_2 generated per volume compared to the expected range of pristine biological enamel, where carbonate is ca. 3–4% by volume (Koch et al., 1997; Elliott, 2002).

4.6. Statistics

Statistical analyses were performed in R. Uncertainty in estimates of $\delta^{18}O_{precip}$ intra-annual range from fossil $\delta^{18}O_{enamel}$ values intra-tooth range includes: (1) uncertainty in the $\delta^{18}O_{enamel}$ intra-tooth range in a fossil collection, (2) uncertainty in the slope of the regression between intra-annual $\delta^{18}O_{precip}$ ranges and intra-tooth $\delta^{18}O_{enamel}$ ranges, and (3) uncertainty in the residuals of the regression between intra-annual $\delta^{18}O_{precip}$ ranges and intra-tooth $\delta^{18}O_{enamel}$ ranges. We propagate these sources of error as the square root of the sum of squares.

5. RESULTS

5.1. Mongolian horse tooth enamel mineralization and oxygen isotopes

Gray levels of inner enamel (40%) are higher at the beginning of the maturation stage than middle (31%) or outer (25%) enamel (Figs. 1 and A.1). The initial mineralization of the entire enamel layer is 32%. Gray levels and estimated mineral content of all layers increase rapidly beyond the level of mature dentine. The maturation length is ca. 20 mm, and outer enamel remains less mineralized than inner and middle enamel. The innermost enamel layer is clearly visible in immature enamel (Fig. A.1) and is more rapidly mineralized compared to other layers of enamel (Blumenthal et al., 2014), but we do not consider this layer further in this study.

Intra-tooth $\delta^{18}O_{enamel}$ profiles were generated with laser ablation for five horse teeth, multiple enamel layers were sampled for three of these teeth, and four of these teeth were also sampled conventionally (Figs. 2 and A.2). The following results are reported in Table A.1, and summarized in Table A.3. The range in $\delta^{18}O_{enamel}$ values for intra-tooth profiles generated with laser ablation for tooth MG-96-518-M3 within inner, middle, and outer layers are 3.8‰, 3.2‰, and 2.4‰, respectively. The range in $\delta^{18}O_{enamel}$ values for intra-tooth profiles generated with laser ablation for tooth MG-96-515-M3 within inner, middle, and outer layers are 5.0‰, 3.6‰, and 2.4‰, respectively, compared to 3.9‰ for the intra-tooth profile generated with conventional sampling. The range in $\delta^{18}O_{enamel}$ values for intra-tooth profiles generated with laser ablation for tooth MG-92-578-M1 within inner and outer layers are 5.0‰ and 3.2‰, respectively, compared to 6.1‰ for the intra-tooth profile generated with conventional sampling. The range in $\delta^{18}O_{enamel}$ values for the intra-tooth profile generated with laser ablation for tooth MG-92-578-M3 within the inner layer is 5.8‰ compared to 4.7‰ for the intra-tooth profile generated with conventional sampling. The range in $\delta^{18}O_{enamel}$ values for the intra-tooth profile generated with laser ablation for tooth MG-92-521-P4 within the middle layer is 5.8‰, and the intra-tooth profile generated with conventional sampling. is 5.8‰. The range in $\delta^{18}O_{enamel}$ values from inner enamel is on average 0.3‰ greater than conventional analysis. The mean range in $\delta^{18}O_{enamel}$ values from all sampled enamel layers with the laser is, on average, 0.4‰ less than conventional analysis. Across all conventionally analyzed horse teeth, including some teeth not analyzed using the laser, the range of intra-tooth $\delta^{18}O$ values vary from 3.4‰ to 6.1‰, and average 4.5 ± 1.1‰ (±1σ) (Fig. A.4). Compared to the annual range in measured $\delta^{18}O_{precip}$ values (20.4‰), conventionally sampled horse intra-tooth $\delta^{18}O_{enamel}$ profiles (4.5‰) preserve 21% of the precipitation signal amplitude. Inner enamel laser ablation intra-tooth $\delta^{18}O$ profiles (4.9‰) preserve 23% of the precipitation signal amplitude.

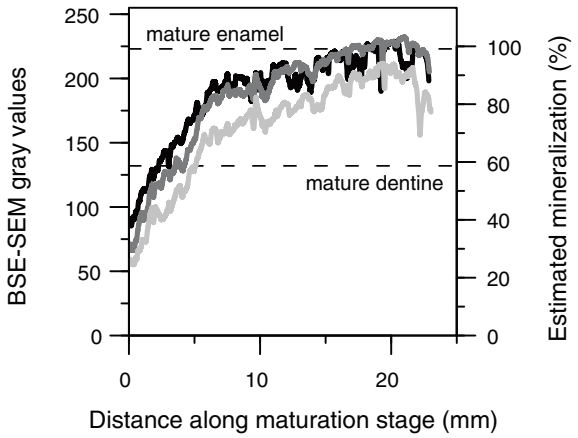

Fig. 1. BSE-SEM gray level transects over the length of maturation of the inner (black), middle (dark gray), and outer (light gray) enamel layers of a horse tooth germ. 100-μm moving averages are used to smooth variability associated with enamel immaturity, cracks, and other surface discontinuities.

5.2. Eastern African precipitation and zebra tooth enamel oxygen isotopes

In tooth collection areas in Kenya and Uganda, modeled $\delta^{18}O_{precip}$ values are highly variable on seasonal scales (Fig. 3). The modeled intra-annual $\delta^{18}O_{precip}$ range across sampled localities in eastern Africa varies from 4.1‰ to 9.2‰. Average intra-tooth $\delta^{18}O_{enamel}$ ranges are 3.5‰

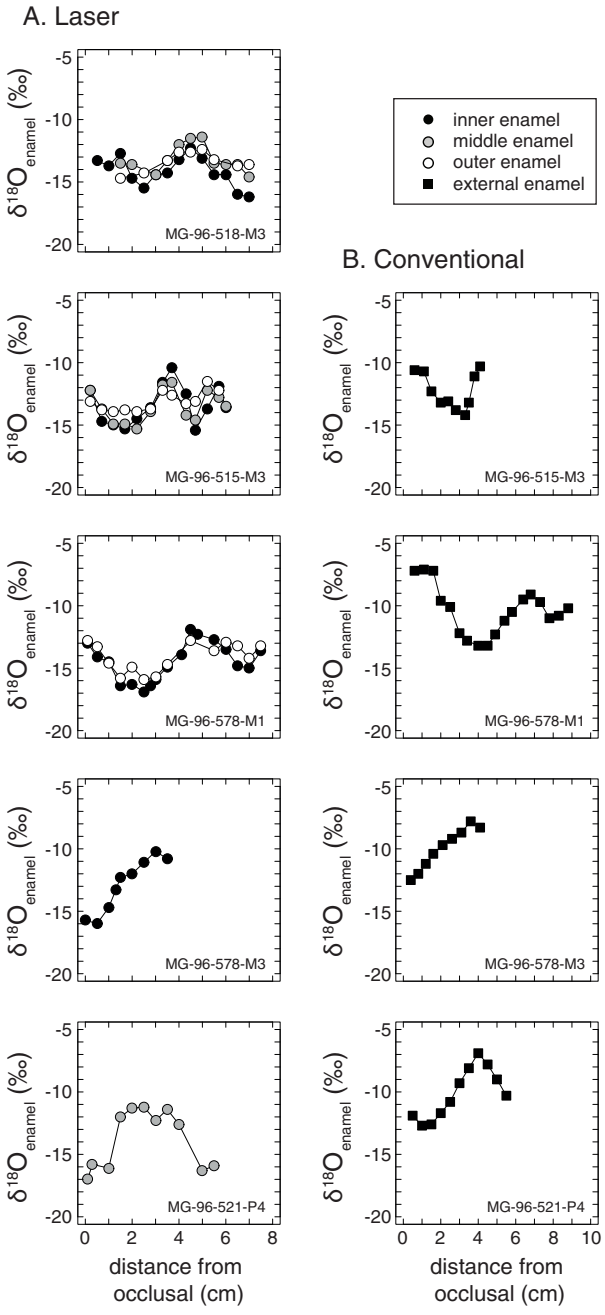

Fig. 2. Intra-tooth oxygen isotope profiles of Mongolian horse teeth using (A) laser ablation and (B) conventional sampling methods.

(Turkana), 2.8‰ (Kidepo), 2.5‰ (Laikipia), 2.3‰ (Lake Mburo), and 2.1‰ (Amboseli). There is a positive, linear relationship ($p < 0.01$, $r^2 = 0.97$) between modeled intra-annual $\delta^{18}O_{precip}$ range and intra-tooth $\delta^{18}O_{enamel}$ range (Fig. 4). We calculate the damping factor (d) with Eq. (1), using the intra-annual range of $\delta^{18}O_{precip}$ values and the mean intra-tooth range of $\delta^{18}O_{enamel}$ values for each sample collection area. Averaged across tooth sampling locations, the damping factor for zebra intra-tooth profiles is 0.54. After correction using this damping factor with Eq. (2), undamped intra-tooth $\delta^{18}O_{enamel}$ ranges are 7.4 ± 2.3‰ (Turkana), 6.1 ± 0.7‰ (Kidepo), 5.5 ± 1.6‰ (Laikipia), 5.0 ± 1.7‰ (Lake Mburo), and 4.1 ± 1.5‰ (Amboseli). Using corrected intra-tooth $\delta^{18}O_{enamel}$ ranges, there is a positive, linear relationship ($p < 0.01$, $r^2 = 0.97$) between modeled intra-annual $\delta^{18}O_{precip}$ range and intra-tooth $\delta^{18}O_{enamel}$ range (Fig. 4). The regression coefficients (slopes and error) of these linear relationships vary significantly from each other ($p < 0.05$, F test). The relationship in Fig. 4 can be inverted to reconstruct intra-annual $\delta^{18}O_{precip}$ variability from corrected fossil intra-tooth $\delta^{18}O_{enamel}$ ranges using the following equation:

$$\delta^{18}O_{precip} = 1.6932 * \delta^{18}O_{enamel} - 3.6357. \quad (3)$$

This statistically significant regression ($p < 0.01$) has a low residual standard error (±0.72‰) and a high coefficient of determination ($r^2 = 0.97$), and as a result this model has sufficient predictive power to address $\delta^{18}O_{precip}$ variability in the fossil record. A power analysis on regressions between intra-tooth $\delta^{18}O_{enamel}$ and intra-annual $\delta^{18}O_{precip}$ variability, assuming $\alpha = 0.05$ and $(1 - \beta) = 0.2$, suggests that between 4 and 5 samples are needed to detect significant differences. The strength of enamel-precipitation relationships ($r^2 > 0.9$) indicates that even small numbers of teeth preserve environmental information, and owing to inherent limitations of tooth collections we accept smaller sample sizes to provide preliminary estimates of isotopic seasonality for periods of fossil preservation.

To understand the significance of seasonal variation in precipitation and tooth enamel, we further consider the relationship between $\delta^{18}O_{precip}$ variability and climate in Africa today. Using a compilation of climate data (WorldClim 2.0) from sites across eastern and central Africa (Table A.2), we find no relationship ($p > 0.05$) between mean annual $\delta^{18}O_{precip}$ and precipitation amount ($p > 0.05$), or between intra-annual $\delta^{18}O_{precip}$ range and precipitation seasonality ($p > 0.05$). We also consider water deficit (or effective rainfall), which describes the difference between evapotranspiration and precipitation and is a useful indicator of water availability in terrestrial vegetated environments in the tropics (Thornthwaite, 1948; Levin et al., 2006; Blumenthal et al., 2017). We find that mean annual $\delta^{18}O_{precip}$ increases with water deficit ($p < 0.001$, $r^2 = 0.32$), and that the intra-annual $\delta^{18}O_{precip}$ range increases with water deficit ($p < 0.02$, $r^2 = 0.15$) (Fig. 5), although these correlations are weak. After excluding sites outside of the equatorial rainfall region, we find that mean annual $\delta^{18}O_{precip}$ decreases with precipitation amount ($p < 0.01$, $r^2 = 0.34$) and increases with water deficit ($p < 0.00001$, $r^2 = 0.72$), and intra-annual $\delta^{18}O_{precip}$ range increases with water deficit ($p < 0.0001$, $r^2 = 0.61$) (Fig. 5). We find no relationship between intra-annual $\delta^{18}O_{precip}$ range and precipitation seasonality ($p > 0.05$).

5.3. Fossil equid tooth enamel oxygen isotopes

The relationship between ranges in intra-tooth $\delta^{18}O_{enamel}$ and intra-annual $\delta^{18}O_{precip}$ values can be used to predict the intra-annual $\delta^{18}O_{precip}$ range in the past. Intra-tooth $\delta^{18}O_{enamel}$ profiles were generated with

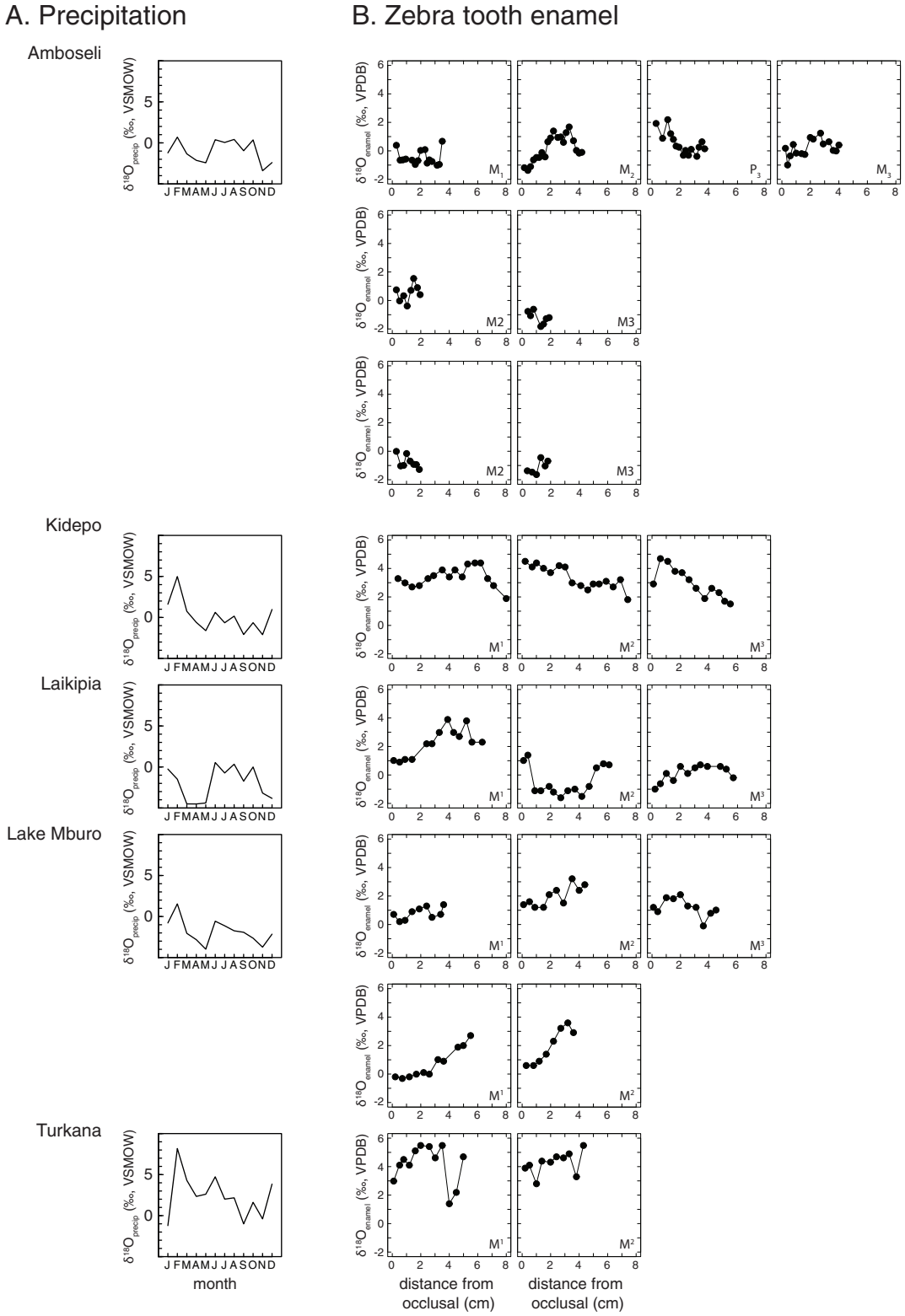

Fig. 3. (A) Modeled oxygen isotopic composition of precipitation. (B) Intra-tooth oxygen isotope variability in zebra teeth. Each row includes teeth from a single individual.

conventional sampling from fossil equid teeth from the Kanjera South Member, including three teeth from bed KS1 and five teeth from bed KS2, and the Kanjera North Member, including one tooth from KN3 (Fig. A.5 and Table A.4). Two additional fossil equid teeth were sampled from the Kasibos Formation (Fig. A.5). The range of

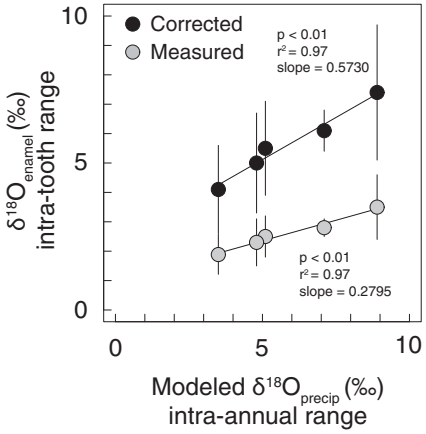

Fig. 4. Relationship between intra-annual range in modeled $\delta^{18}O$ values of precipitation and intra-tooth range in $\delta^{18}O$ values of zebra cheek teeth.

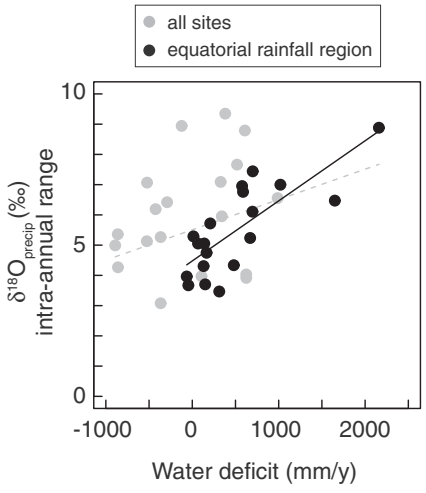

Fig. 5. Water deficit (WD) and intra-annual range in modeled $\delta^{18}O$ values of precipitation across all sites (gray) and sites located in the bimodal equatorial rainfall region (black).

intra-tooth $\delta^{18}O_{enamel}$ values are $2.5 \pm 0.5‰$ (KS1), $1.9 \pm 0.5‰$ (KS2), 1.8‰ (KN3), and $1.8 \pm 0.3‰$ (Kasibos). After correction using the damping factor and propagating error, average intra-tooth $\delta^{18}O_{enamel}$ ranges are $5.4 \pm 0.7‰$ (KS1), $4.1 \pm 0.7‰$ (KS2), $3.9 \pm 0.5‰$ (KN3), and $4.0 \pm 0.5‰$ (Kasibos) (Table A.5). For comparison we also use previously published oxygen isotope data for fossil equid teeth from Olduvai Bed II, including 2 teeth from sediments stratigraphically positioned between Tuff IIA and IIB (Interval IIA), and 1 tooth from sediments stratigraphically positioned between Tuff IIB and IIC (Interval IIB) (Uno et al., 2018). The range of intra-tooth $\delta^{18}O_{enamel}$ values are 2.7‰ (Interval IIA) and $1.4 \pm 0.0‰$ (Interval IIB). After correction using the damping factor, intra-tooth $\delta^{18}O_{enamel}$ ranges are $5.9 \pm 0.5‰$ (Interval IIA) and $3.0 \pm 0.5‰$ (Interval IIB). Previously published oxygen isotope data for 2 fossil equid teeth from Manyara Beds include 2 specimens from site MK4 (Wolf et al., 2010). The range of intra-tooth $\delta^{18}O_{enamel}$ values is $1.5 \pm 1.3‰$, and $3.1 \pm 2.9‰$ after correction using the damping factor. Intra-annual $\delta^{18}O_{precip}$ ranges in the Pleistocene, estimated from corrected fossil intra-tooth $\delta^{18}O_{enamel}$ ranges, resemble intra-annual $\delta^{18}O_{precip}$ variation in modern eastern African environments, bounded by Turkana and Amboseli in our modern dataset (Fig. 6 and Table A.2). We find no trend over time ($p > 0.05$) for fossil collections included here in southern Kenya and northern Tanzania, although additional specimens and sites are needed to address this issue in a meaningful way. The similar isotopic range in fossil compared to modern equid teeth ($\delta^{18}O_{enamel}$ range >1‰) suggests that diagenetic alteration has not homogenized the oxygen isotopic composition of these fossils.

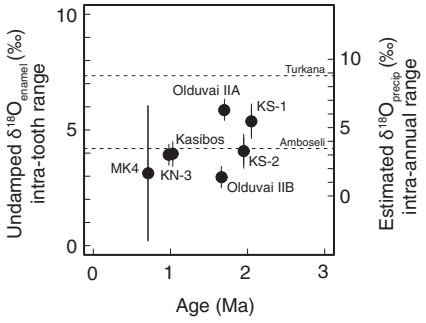

Fig. 6. Intra-tooth range in $\delta^{18}O$ values of fossil equid cheek teeth. Dotted lines represent intra-annual range in modeled $\delta^{18}O$ values of precipitation from Turkana, Kenya and Serengeti, Tanzania, for reference. Uncertainty represents the propagated error of estimated $\delta^{18}O_{precip}$ intra-annual range.

6. DISCUSSION

6.1. *In situ* microsampling of tooth enamel

These results demonstrate that *in situ* laser ablation (LA-GC-IRMS) analysis can be used to generate intra-tooth profiles within discrete layers of large mammal tooth enamel. Oxygen isotope time-series in Mongolian horse teeth record the $\delta^{18}O_{enamel}$ shift associated with seasonal climate, although signal amplitude in intra-tooth $\delta^{18}O_{enamel}$ values was blurred compared to intra-annual $\delta^{18}O_{precip}$ values (Figs. 2 and A.4). The intra-tooth $\delta^{18}O_{enamel}$ range from inner enamel is greater than middle and outer enamel profiles by 1.0‰ and 1.9‰, respectively, consistent with mammalian tooth enamel maturation patterns presented here (Fig. 1) and elsewhere (Blumenthal et al., 2014). Thus, targeting inner enamel provides less blurred signal amplitudes compared to middle and outer enamel layers, as previously demonstrated (Zazzo et al., 2005). Innermost enamel may provide even greater gains in signal amplitude (Blumenthal et al., 2014), although this has not yet been tested in large mammal teeth and lies beyond the scope of this study. Despite observing reduced signal blurring in inner enamel, we unexpectedly find that laser ablation does not provide greater intra-tooth signal amplitude compared

to conventional sampling. The difference in intra-tooth $\delta^{18}O_{enamel}$ range from inner enamel and conventional profiles is small (0.3‰), and intra-tooth $\delta^{18}O_{enamel}$ ranges from middle and outer enamel profiles are smaller than conventional profiles by 0.5‰ and 2.0‰, respectively. Thus, inner enamel provides signal amplitude similar to conventional sampling, while other layers preserve more highly blurred signals.

The failure to recover a less blurred signal in inner enamel using laser ablation compared to conventional sampling is unexpected because hand drilled sample grooves likely vary in depth and preferentially include outer and middle enamel layers, potentially mixing enamel from different maturation time intervals (Zazzo et al., 2005). The mineralization front in equid teeth appears to follow a high angle to the EDJ, roughly perpendicular to the outer enamel surface (Fig. A.1) (Trayler and Kohn, 2017), suggesting only minor signal blurring from enamel layer mixing in this study. Mixing enamel layers may pose a greater problem in cases where enamel maturation is more spatially complex, such as the wedge-shaped pattern observed in cow teeth (Trayler and Kohn, 2017).

Our finding that inner enamel sampling does not improve upon conventional sampling also contrasts with the conclusions of previous studies isolating inner enamel in bovid (Zazzo et al., 2005), proboscidean (Metcalfe and Longstaffe, 2012), and rodent (Blumenthal et al., 2014) teeth. However, in the proboscidean study other enamel layers were not sampled for comparison with inner enamel (Metcalfe and Longstaffe, 2012), and the bovid study relied largely on model predictions and presented few inner enamel isotope measurements (Zazzo et al., 2005). In the rodent study, inner enamel was sampled using secondary ion mass spectrometry (SIMS) and the outer enamel surface was sampled using laser ablation, both targeting bulk enamel (Blumenthal et al., 2014).

The comparison between laser ablation and conventional sampling may be complicated by the analysis of different oxygen-bearing phases of enamel. The majority of oxygen in bulk enamel resides in phosphate, and phosphate oxygen appears to retain either less blurred (Pellegrini et al., 2011) or similarly blurred (Trayler and Kohn, 2017) intra-tooth signals; thus, finding greater signal amplitude in carbonate compared to (mostly phosphate) bulk enamel is unexpected. Differences in the timing and routing of mineral uptake and oxygen isotope incorporation in carbonate versus phosphate components (Pellegrini et al., 2011) could result in additional signal blurring in bulk enamel compared to individual components. Isolating inner enamel carbonate using micromilling may provide a more effective comparison to conventional sampling (Zazzo et al., 2005; Metcalfe and Longstaffe, 2012; Trayler and Kohn, 2017). These observations indicate that novel microsampling techniques with high spatial resolution for targeting discrete enamel layers or minimizing spot size is not always effective for reducing signal attenuation. Conventional sampling methods remain preferred for routine measurements of intra-tooth isotopic variability in large mammals for a wide range of applications (Trayler and Kohn, 2017; Green et al., 2018b).

6.2. Climate and equid tooth enamel oxygen isotopes in eastern Africa

Our findings indicate that changes in intratooth isotopic variation can be used to address past precipitation isotopic seasonality. The correspondence between $\delta^{18}O_{enamel}$ variability and $\delta^{18}O_{precip}$ variability among extant zebra in eastern Africa (Fig. 4) can be explained by the water-dependence of zebras, which today are restricted by the distribution of permanent water sources (Western, 1975; Sitters et al., 2009; Ogutu et al., 2010) such that the isotopic composition of body water and enamel reflects variation in environmental waters (Bryant et al., 1994; Huertas et al., 1995; Sharp and Cerling, 1998; Hoppe et al., 2005; Levin et al., 2006; Blumenthal et al., 2017). We find that isotopic seasonality relates to rainfall amount and aridity in the present-day equatorial rainfall region of eastern Africa (Fig. 5), suggesting that the amount effect represents a useful model for understanding climatological control of isotopic seasonality in this areas, as observed elsewhere in the tropics (Bowen, 2008). The amount effect relates to a number of different processes, including re-evaporation of rain and exchange with surrounding vapor, recycling of vapor in the subcloud layer by convective flux, intensity of convective storms and rainout of air mass moisture, and precipitation of vapor formed by evapotranspiration near the land surface or evaporation of surface waters (Dansgaard, 1964; Rozanski et al., 1993; Araguás-Araguá et al., 2000; Risi et al., 2008).

Under the assumption that the distribution and isotopic composition of source waters have not changed over geologic time, equid tooth $\delta^{18}O_{enamel}$ variability could conceivably be used to infer seasonal aridity in this region in the past. However, when considering the whole of eastern Africa including areas outside of the equatorial rainfall region, influences on isotopic seasonality include hydroclimatic processes unrelated to humidity, such as precipitation microphysics, cloud type, and moisture transport (Konecky et al., 2019). Additionally, past climatic and hydrological change, such as Pliocene-Pleistocene variation in tropical sea surface temperatures (Wara et al., 2005; Herbert et al., 2010; Liddy et al., 2016) or more recent migrations of the Congo Air Boundary (Costa et al., 2014; Junginger et al., 2014), indicate that influences on isotopic variation of precipitation likely shifted over time. Given such uncertainties in the climatological controls on isotopic seasonality in eastern Africa, and past changes in these controls, we use fossil tooth isotopic records to discuss past isotopic seasonality but refrain from quantifying past seasonality aridity.

There are additional uncertainties in interpreting isotopic variation in equid teeth. First, isotopic variability among teeth within a fossil collection necessarily integrates environmental inputs over the duration of fossil preservation, which may have included changes in seasonality patterns. Even where fossil collections represent discrete, geologically brief intervals of time, such as archaeological levels, it is not possible to link individual fossils to particular millennial or sub-millennial climate cycles. Additionally, teeth along the tooth row represent different periods of

growth such that even teeth from the same individual would not perfectly overlap in time, and would record different isotopic signals. Finally, even individuals living in the same time and place may vary isotopically, as demonstrated by isotopic variation of body water among sheep consuming the same food and water under controlled conditions (Green et al., 2018a), suggesting some degree of baseline isotopic variability driven by inter-individual behavioral, physiological, and/or genetic variability.

Second, we cannot address aspects of the frequency and duration of seasons, which are not clearly preserved in intra-tooth $\delta^{18}O_{enamel}$ profiles among modern zebra (Fig. 3). This issue stems from general difficulties in interpreting signal structure in intra-tooth $\delta^{18}O_{enamel}$ profiles, which can be altered substantially from primary environmental signals primarily due to enamel maturation (Passey et al., 2005; Green et al., 2018b). Inversion modeling may be useful for investigating the structure of seasonal-scale signals (i.e. unimodal vs bimodal rainfall seasonality) from intra-tooth isotopic records, although relating signal structure of intra-tooth records even after inversion is not straightforward, owing to variability in drinking behavior or physiology. For instance, for a mammal in the tropics low and high $\delta^{18}O_{enamel}$ values would normally be interpreted as wet and dry seasons, respectively, but the timing and duration of seasons could be misidentified depending on seasonal patterns of water intake from plants (higher $\delta^{18}O$) and permanent water sources (lower $\delta^{18}O$). Additionally, the oxygen isotopic composition of leaf water and cellulose of plants vary with humidity, although leaf water enrichment over source water is not always equivalent between C_3 and C_4 plants (Helliker and Ehleringer, 2002). In eastern Africa, equids have consistently C_4 grass-dominated diets since the late Miocene (Uno et al., 2011), minimizing potential bias, if any, from seasonally switching between C_3 and C_4 resources when analyzing fossil equids in this region.

Third, movement over the landscape, associated with the distribution of food, water, and predators (Bracis and Mueller, 2017; Alerstam and Bäckman, 2018), could also lead to modified intra-tooth isotopic signals. Zebras present the particular problem of long-distance migrations, although it is not possible to know to what extent past movements resemble the migratory behavior of extant populations. Future strontium isotope studies may be able to address past movement patterns of mammals in eastern Africa, as demonstrated in other regions (Copeland et al., 2016; Lehmann et al., 2018; Wallace et al., 2019). In sum, more work is needed to understand behavioral and environmental correlates of intra-tooth isotopic variability in wild mammals.

6.3. Paleoclimate and hominin environments

Our tooth enamel records demonstrate variable isotopic seasonality, likely reflecting seasonal changes in moisture amount or source, during periods of fossil preservation in southwestern Kenya and northern Tanzania in the Early Pleistocene. These findings are consistent with the notion that climate variability was an important feature of past environments in Africa, including seasonal cycles superimposed on longer suborbital and orbital cycles (Potts, 2013; Levin, 2015; Potts and Faith, 2015). There is abundant geologic evidence from marine (Rossignol-Strick, 1983; Tiedemann et al., 1994; Larrasoaña et al., 2003; deMenocal, 2004; Trauth et al., 2009; Rose et al., 2016) and continental records (Deino et al., 2006; Ashley, 2007; Kingston et al., 2007; Trauth et al., 2007; Lepre et al., 2007; Joordens et al., 2011; Deocampo et al., 2017; Lupien et al., 2018; Hopley et al., 2018) for moisture cycling with orbital periodicities, suggesting that solar insolation change was a primarily driver of paleoclimatic change across Africa. Orbital precession (19–23 kyr cycles) influences the seasonal distribution of insolation in the tropics, which manifests as variation in rainfall seasonality (Clement et al., 2004; Kingston, 2005; Berger et al., 2006; Merlis et al., 2013), indicating a potential link between climatic variability across time scales.

We find no long-term trend in isotopic seasonality in southern Kenya and northern Tanzania from ca. 2.0 Ma to ca. 0.7 Ma (Fig. 6), indicating no long-term change in seasonal aridity, moisture source, or other hydroclimate controls on isotopic seasonality. The lack of long-term aridification would be consistent with tooth enamel and leaf wax biomarker records in Turkana, northern Kenya (Blumenthal et al., 2017; Lupien et al., 2018), indicating diversity in how basins respond to continental-scale aridification (Levin, 2015). On the other hand, paleosol carbonate $\delta^{18}O$ values in Olduvai (Cerling and Hay, 1986; Sikes, 1994; Sikes and Ashley, 2007) and Turkana (Cerling and Hay, 1986; Levin et al., 2011) basins increase after ~2.0 Ma, which could reflect increasing aridity, or changes in basin hydrology, soil water evaporation, and vegetation. These factors can influence carbonate $\delta^{18}O$ and tooth enamel $\delta^{18}O$ records in different ways, complicating inter-proxy comparisons even if both reflect meteoric waters generally (Levin et al., 2011; Blumenthal et al., 2017). We do not address the possibility of aridification prior to 2.0 Ma, which may be an important feature of late Miocene and early Pliocene climatic change (Liddy et al., 2016; Fortelius et al., 2016).

Isotopic seasonality can also be influenced by large lakes, which are a common feature of many rift basins in eastern Africa throughout the Pliocene and Pleistocene (Trauth et al., 2005; Maslin et al., 2014), particularly in cases where distinct mesoscale circulation systems alter seasonal precipitation patterns, as in the present-day Lake Victoria Basin (Yin et al., 2000; Sun et al., 2015). Kanjera and Kasibos Formation sediments are located in close geographical vicinity to modern Lake Victoria, and Kanjera North Member sediments (including KN3) indicate the presence of a nearby lake, but the ancient lake was small and likely unrelated to the present-day lake (Behrensmeyer et al., 1995) that is thought to be middle or late Pleistocene in age (Kent, 1944; Doornkamp and Temple, 1966; Meyer et al., 1990; Johnson et al., 1996; Danley et al., 2012). Paleolake Olduvai repeatedly expanded and contracted during the early Pleistocene, including lower Bed II, but was likely too small to influence atmospheric circulation (Hay and Kyser, 2001; Ashley et al., 2010; Stanistreet et al., 2018).

Our findings suggest that Early Pleistocene hominins inhabited environments that were seasonally variable to an extent similar to climates in present-day eastern Africa. In the tropics today, rainfall seasonality influences vegetation and animal communities, suggesting that selective pressures associated with seasonal changes in the abundance and distribution of resources may have been important drivers of hominin evolution (Foley, 1993; Kingston, 2007; Trauth et al., 2007; Macho and Leakey, 2009; Potts and Faith, 2015), consistent with isotopic and histological evidence for seasonal-scale variation in diet and environmental conditions (Macho et al., 1996, 2003; Sponheimer et al., 2006; Lee-Thorp et al., 2010).

Equid teeth from Olduvai and Kanjera South indicate higher isotopic seasonality in stratigraphically lower strata (Olduvai IIA and KS1, respectively) and lower isotopic seasonality in the succeeding strata (Olduvai IIB and KS2). That isotopic seasonality varied over relatively short periods of time indicates that these hominins were able to accommodate significant shifts in seasonality, consistent with previous studies at Olduvai demonstrating short-term environmental variability on orbital and suborbital time scales (Liutkus et al., 2005; Ashley, 2007; Deocampo et al., 2017; Colcord et al., 2018). Despite shifts in isotopic seasonality, paleovegetation and mammal paleodiet proxies indicate relatively stable ecological conditions, including a C_4 grass-dominated savanna biome (woody cover from 3% to 42%) with small areas of denser cover during lower Bed II times at Olduvai (Bamford et al., 2006; Uno et al., 2018; de la Torre et al., 2018; Bibi et al., 2018) and a C_4-dominated grassland (woody cover <10%) at Kanjera South (Plummer et al., 2009a; Plummer et al., 2009b; Cerling et al., 2015). The presence of archaeological traces in the Kanjera and Kasibos Formations (Plummer, 1991; Ditchfield et al., 1999; Plummer and Bishop, 2016), Olduvai Bed II (de la Torre et al., 2018), and Manyara Beds (Kaiser et al., 2010), suggests no preference for isotopic seasonality. The archaeological levels at Kanjera South and Olduvai preserve particularly rich records of Early Stone Age hominin behavior, including selective use and transport of lithic raw materials, repeated primary access to mammal carcasses, and the exploitation of a diversity of plant resources including underground storage organs (Ferraro et al., 2013; Lemorini et al., 2014; Arroyo and de la Torre, 2018; McHenry and de la Torre, 2018; Pante et al., 2018). This suite of behaviors suggests that by the Early Pleistocene toolmaking hominins were omnivorous and relied on stone tool-dependent foraging within variably seasonal environments.

7. CONCLUSIONS

These findings demonstrate that *in situ* sampling with laser ablation is useful for investigating the relationships between enamel maturation and isotopic variability in large mammalian herbivore teeth, but may not be ideal for widespread use because it does not effectively remove signal blurring compared to conventional sampling methods. Equid intra-tooth variability in enamel $\delta^{18}O$ reflects intra-annual variability in precipitation $\delta^{18}O$, representing a proxy for past change in isotopic seasonality, although the frequency and duration of seasons are not clearly preserved. Pleistocene fossil equid teeth from southern Kenya and northern Tanzania indicate past isotopic seasonality similar to modern eastern African climates. Addressing the link between long-term changes in seasonality and other environmental changes, such as the expansion of C_4 plants, requires additional intra-tooth $\delta^{18}O$ records from the late Miocene and Pliocene and from additional basins. Finally, additional modern datasets are needed to test the validity of this approach in other taxa and in regions outside of tropical eastern Africa.

ACKNOWLEDGEMENTS

We thank individuals and organizations who provided assistance with sample collection, including Anna K. Behrensmeyer, Frederick Lala Odock, Erustus Kanga, the Kenya Wildlife Service, and the Uganda Wildlife Authority. We thank Linda Ayliffe for assistance in the laboratory, and to Kevin Uno for sharing raw data. This research was funded by the Leakey Foundation, National Geographic Society (8784-10 and 9349-13), The National Science Foundation (1260535), the Packard Foundation, and the Wenner-Gren Foundation (8694). Thanks also to Fred Longstaffe and two anonymous reviewers for comments on a previous draft.

APPENDIX A. SUPPLEMENTARY MATERIAL

Supplementary data to this article can be found online at https://doi.org/10.1016/j.gca.2019.06.037.

REFERENCES

Aggarwal P. K., Choudhry M. A., Eder S., Hofko S., Izewski E., Kurttas T. and Terzer S. (2008) *Atlas of Isotope Hydrology – Asia and the Pacific*. IAEA, Austria.

Alerstam T. and Bäckman J. (2018) Ecology of animal migration. *Curr. Biol.* **28**, R968–R972.

Antón S. C., Potts R. and Aiello L. C. (2014) Evolution of early Homo: an integrated biological perspective. *Science* **345**, 1236828.

Aoba T. and Moreno E. C. (1990) Changes in the nature and composition of enamel mineral during procine amelogenesis. *Calcif. Tissue Int.* **47**, 356–364.

Araguás-Araguá L., Froehlich K. and Rozanski K. (2000) Deuterium and oxygen-18 isotope composition of precipitation and atmospheric moisture. *Hydrol. Process.* **14**, 1341–1355.

Archibald S. and Hempson G. P. (2016) Competing consumers: contrasting the patterns and impacts of fire and mammalian herbivory in Africa. *Philos. Trans. R. Soc. Lond. B Biol. Sci.* **371**, 20150309.

Arroyo A. and de la Torre I. (2018) Pounding tools in HWK EE and EF-HR (Olduvai Gorge, Tanzania): percussive activities in the Oldowan-Acheulean transition. *J. Hum. Evol.* **120**, 402–421.

Ashley G. (2007) Orbital rhythms, monsoons, and playa lake response, Olduvai Basin, equatorial East Africa (ca. 1.85–1.74 Ma). *Geology* **35**, 1091–1094.

Ashley G. M., Dominguez-Rodrigo M., Bunn H. T., Mabulla A. Z. P. and Baquedano E. (2010) Sedimentary geology and human origins: a fresh look at Olduvai Gorge Tanzania. *J. Sediment. Res.* **80**, 703–709.

Bahloul K., Pereladova O. B., Soldatova N., Fisenko G., Sidorenko E. and Sempéré A. J. (2001) Social organization

and dispersion of introduced kulans (*Equus hemionus kulan*) and Przewalski horses (*Equus przewalski*) in the Bukhara Reserve Uzbekistan. *J. Arid Environ.* **47**, 309–323.

Balasse M. (2002) Reconstructing dietary and environmental history from enamel isotopic analysis: time resolution of intra-tooth sequential sampling. *Int. J. Osteoarchaeol.* **12**, 155–165.

Balasse M. (2003) Potential biases in sampling design and interpretation of intra-tooth isotope analysis. *Int. J. Osteoarchaeol.* **13**, 3–10.

Bamford M. K., Albert R. M. and Cabanes D. (2006) Plio-Pleistocene macroplant fossil remains and phytoliths from Lowermost Bed II in the eastern palaeolake margin of Olduvai Gorge Tanzania. *Quat. Int.* **148**, 95–112.

Bamford M. K., Senut B. and Pickford M. (2013) Fossil leaves from Lukeino, a 6-million-year-old Formation in the Baringo Basin Kenya. *Geobios Mem. Spec.* **46**, 253–272.

Barker P. A., Hurrell E. R., Leng M. J., Wolff C., Cocquyt C., Sloane H. J. and Verschuren D. (2011) Seasonality in equatorial climate over the past 25 k.y. revealed by oxygen isotope records from Mount Kilimanjaro. *Geology* **39**, 1111–1114.

Behrensmeyer A. K. (1978) Taphonomic and ecologic information from bone weathering. *Paleobiology* **4**, 150–162.

Behrensmeyer A. K., Potts R., Plummer T., Tauxe L., Opdyke N. and Jorstad T. (1995) The Pleistocene locality of Kanjera, Western Kenya: stratigraphy, chronology and paleoenvironments. *J. Hum. Evol.* **29**, 247–274.

Bendrey R., Vella D., Zazzo A., Balasse M. and Lepetz S. (2015) Exponentially decreasing tooth growth rate in horse teeth: implications for isotopic analyses. *Archaeometry* **57**, 1104–1124.

Beniash E., Metzler R. A., Lam R. S. K. and Gilbert P. U. P. A. (2009) Transient amorphous calcium phosphate in forming enamel. *J. Struct. Biol.* **166**, 133–143.

Berger A., Loutre M. F. and Mélice J. L. (2006) Equatorial insolation: from precession harmonics to eccentricity frequencies. *Clim. Past* **2**, 131–136.

Bernard A., Daux V., Lécuyer C. and Brugal J.-P. (2009) Pleistocene seasonal temperature variations recorded in the $\delta^{18}O$ of *Bison priscus* teeth. *Earth Planet. Sci. Lett.* **283**, 133–143.

Bibi F., Pante M., Souron A., Stewart K., Varela S., Werdelin L., Boisserie J.-R., Fortelius M., Hlusko L., Njau J. and de la Torre I. (2018) Paleoecology of the Serengeti during the Oldowan-Acheulean transition at Olduvai Gorge, Tanzania: The mammal and fish evidence. *J. Hum. Evol.* **120**, 48–75.

Bloebaum R. D., Skedros J. G., Vajda E. G., Bachus K. N. and Constantz B. R. (1997) Determining mineral content variations in bone using backscattered electron imaging. *Bone* **20**, 485–490.

Blumenthal S. A., Chritz K. L., Cerling T. E., Bromage T. G., Kozdon R. and Valley J. W. (2014) Stable isotope time-series in mammalian teeth: *In situ* $\delta^{18}O$ from the innermost enamel layer. *Geochim. Cosmochim. Acta* **124**, 223–236.

Blumenthal S. A., Levin N. E., Brown F. H., Brugal J.-P., Chritz K. L., Harris J. M., Jehle G. E. and Cerling T. E. (2017) Aridity and hominin environments. *Proc. Natl. Acad. Sci. U. S. A.* **114**, 7331–7336.

Bocherens H., Mashkour M., Billiou D., Pellé E. and Mariotti A. (2001) A new approach for studying prehistoric herd management in arid areas: intra-tooth isotopic analyses of archaeological caprine from Iran. *Comptes Rendus de l'Académie des Sciences – Series IIA – Earth Planet. Sci.* **332**, 67–74.

Bowen G. J. (2008) Spatial analysis of the intra-annual variation of precipitation isotope ratios and its climatological corollaries. *J. Geophys. Res.* **113**, D05113.

Bowen G. J. and Revenaugh J. (2003) Interpolating the isotopic composition of modern meteoric precipitation. *Water Resour. Res.* **39**, 1299.

Boyde A., Jones S. J., Aerssens J. and Dequeker J. (1995) Mineral density quantitation of the human cortical iliac crest by backscattered electron image analysis: variations with age, sex, and degree of osteoarthritis. *Bone* **16**, 619–627.

Bracis C. and Mueller T. (2017) Memory, not just perception, plays an important role in terrestrial mammalian migration. *Proc. Biol. Sci.* **284**.

Bryant J. D. and Froelich P. N. (1995) A model of oxygen isotope fractionation in body water of large mammals. *Geochim. Cosmochim. Acta* **59**, 4523–4537.

Bryant J. D., Luz B. and Froelich P. N. (1994) Oxygen isotopic composition of fossil horse tooth phosphate as a record of continental paleoclimate. *Palaeogeogr. Palaeoclimatol. Palaeoecol.* **107**, 303–316.

Bryant J. D., Koch P. L., Froelich P. N., Showers W. J. and Genna B. J. (1996) Oxygen isotope partitioning between phosphate and carbonate in mammalian apatite. *Geochim. Cosmochim. Acta* **60**, 5145–5148.

Camberlin P. and Planchon O. (1997) Coastal precipitation regimes in Kenya. *Geogr. Ann. Ser. A. Phys. Geogr.* **79**, 109–119.

Camberlin P., Boyard-Micheau J., Philippon N., Baron C., Leclerc C. and Mwongera C. (2014) Climatic gradients along the windward slopes of Mount Kenya and their implication for crop risks. Part 1: climate variability. *Int. J. Climatol.* **34**, 2136–2152.

Cerling T. E. and Sharp Z. D. (1996) Stable carbon and oxygen isotope analysis of fossil tooth enamel using laser ablation. *Palaeogeogr. Palaeoclimatol. Palaeoecol.* **126**, 173–186.

Cerling T. E. and Hay R. L. (1986) An isotopic study of paleosol carbonates from Olduvai Gorge. *Quat. Res.* **25**, 63–78.

Cerling T. E., Harris J. M., Hart J. A., Kaleme P., Klingel H., Leakey M. G., Levin N. E., Lewison R. L. and Passey B. H. (2008) Stable isotope ecology of the common hippopotamus. *J. Zool.* **276**, 204–212.

Cerling T. E., Brown F. H. and Wynn J. (2015) On the environment of aramis. *Curr. Anthropol.* **55**, 469–470.

Cerling T. E. and Harris J. M. (1999) Carbon isotope fractionation between diet and bioapatite in ungulate mammals and implications for ecological and paleoecological studies. *Oecologia* **120**, 347–363.

Cernusak L. A., Barbour M. M., Arndt S. K., Cheesman A. W., English N. B., Feild T. S., Helliker B. R., Holloway-Phillips M. M., Holtum J. A. M., Kahmen A., McInerney F. A., Munksgaard N. C., Simonin K. A., Song X., Stuart-Williams H., West J. B. and Farquhar G. D. (2016) Stable isotopes in leaf water of terrestrial plants. *Plant Cell Environ.* **39**, 1087–1102.

Clement A. C., Hall A. and Broccoli A. J. (2004) The importance of precessional signals in the tropical climate. *Clim. Dyn.* **22**, 327–341.

Clementz M. T. (2012) New insight from old bones: stable isotope analysis of fossil mammals. *J. Mammal.* **93**, 368–380.

Codron J., Codron D., Sponheimer M., Kirkman K., Duffy K. J., Raubenheimer E. J., Mélice J.-L., Grant R., Clauss M. and Lee-Thorp J. A. (2012) Stable isotope series from elephant ivory reveal lifetime histories of a true dietary generalist. *Proc. Biol. Sci.* **279**, 2433–2441.

Colcord D. E., Shilling A. M., Sauer P. E., Freeman K. H., Njau J. K., Stanistreet I. G., Stollhofen H., Schick K. D., Toth N. and Brassell S. C. (2018) Sub-Milankovitch paleoclimatic and paleoenvironmental variability in East Africa recorded by Pleistocene lacustrine sediments from Olduvai Gorge Tanzania. *Palaeogeogr. Palaeoclimatol. Palaeoecol.* **495**, 284–291.

Copeland S. R., Cawthra H. C., Fisher E. C., Lee-Thorp J. A., Cowling R. M., le Roux P. J., Hodgkins J. and Marean C. W. (2016) Strontium isotope investigation of ungulate movement patterns on the Pleistocene Paleo-Agulhas Plain of the Greater Cape Floristic Region, South Africa. *Quat. Sci. Rev.* **141**, 65–84.

Costa K., Russell J., Konecky B. and Lamb H. (2014) Isotopic reconstruction of the African Humid Period and Congo Air Boundary migration at Lake Tana Ethiopia. *Quat. Sci. Rev.* **83**, 58–67.

Crowell-Davis S. L., Houpt K. A. and Carnevale J. (1985) Feeding and drinking behavior of mares and foals with free access to pasture and water. *J. Anim. Sci.* **60**, 883–889.

D'Ambrosia A. R., Clyde W. C., Fricke H. C. and Chew A. E. (2014) Stable isotope patterns found in early Eocene equid tooth rows of North America: Implications for reproductive behavior and paleoclimate. *Palaeogeogr. Palaeoclimatol. Palaeoecol.* **414**, 310–319.

Danley P. D., Husemann M., Ding B., Dipietro L. M., Beverly E. J. and Peppe D. J. (2012) The impact of the geologic history and paleoclimate on the diversification of East African cichlids. *Int. J. Evol. Biol.* **2012**, 574851.

Dansgaard W. (1964) Stable isotopes in precipitation. *Tellus* **16**, 436–468.

de la Torre I., Albert R. M., Macphail R., McHenry L. J., Pante M. C., Rodríguez-Cintas Á., Stanistreet I. G. and Stollhofen H. (2018) The contexts and early Acheulean archaeology of the EF-HR paleo-landscape (Olduvai Gorge, Tanzania). *J. Hum. Evol.* **120**, 274–297.

de Leeuw J., Waweru M. N., Okello O. O., Maloba M., Nguru P., Said M. Y., Aligula H. M., Heitkönig I. M. A. and Reid R. S. (2001) Distribution and diversity of wildlife in northern Kenya in relation to livestock and permanent water points. *Biol. Conserv.* **100**, 297–306.

de Winter N. J., Snoeck C. and Claeys P. (2016) Seasonal cyclicity in trace elements and stable isotopes of modern horse enamel. *PLoS One* **11**, e0166678.

Deino A. L., Kingston J. D., Glen J. M., Edgar R. K. and Hill A. (2006) Precessional forcing of lacustrine sedimentation in the late Cenozoic Chemeron Basin, Central Kenya Rift, and calibration of the Gauss/Matuyama boundary. *Earth Planet. Sci. Lett.* **247**, 41–60.

deMenocal P. B. (2004) African climate change and faunal evolution during the Pliocene-Pleistocene. *Earth Planet. Sci. Lett.* **220**, 3–24.

Deocampo D. M., Berry P. A., Beverly E. J., Ashley G. M. and Jarrett R. E. (2017) Whole-rock geochemistry tracks precessional control of Pleistocene lake salinity at Olduvai Gorge, Tanzania: a record of authigenic clays. *Geology* **45**, 683–686.

di Lernia S., Tafuri M. A., Gallinaro M., Alhaique F., Balasse M., Cavorsi L., Fullagar P. D., Mercuri A. M., Monaco A., Perego A. and Zerboni A. (2013) Inside the "African Cattle Complex": Animal burials in the Holocene Central Sahara. *PLoS One* **8**, e56879.

Diez-Martín F., Sánchez Yustos P., Uribelarrea D., Baquedano E., Mark D. F., Mabulla A., Fraile C., Duque J., Díaz I., Pérez-González A., Yravedra J., Egeland C. P., Organista E. and Domínguez-Rodrigo M. (2015) The origin of the acheulean: The 1.7 million-year-old site of FLK West, Olduvai Gorge (Tanzania). *Sci. Rep.* **5**, 17839.

Ditchfield P., Hicks J., Plummer T., Bishop L. C. and Potts R. (1999) Current research on the late Pliocene and Pleistocene deposits north of Homa Mountain, southwestern Kenya. *J. Hum. Evol.* **36**, 123–150.

Ditchfield P. W., Whitfield E., Vincent T., Plummer T., Braun D., Deino A., Hertel F., Oliver J. S., Louys J. and Bishop L. C. (2018) Geochronology and physical context of Oldowan site formation at Kanjera South, Kenya. *Geological Magazine*, 1–11.

Doornkamp J. C. and Temple P. H. (1966) Surface, Drainage and Tectonic Instability in Part of Southern Uganda. *Geogr. J.* **132**, 238–252.

Elliott J. C. (2002) Calcium phosphate biominerals. *Rev. Mineral. Geochem.* **48**, 427–453.

Elliott J. C., Holcomb D. W. and Young R. A. (1985) Infrared determination of the degree of substitution of hydroxyl by carbonate ions in human dental enamel. *Calcif. Tissue Int.* **37**, 372–375.

Fabre M., Lécuyer C., Brugal J.-P., Amiot R., Fourel F. and Martineau F. (2011) Late Pleistocene climatic change in the French Jura (Gigny) recorded in the $\delta^{18}O$ of phosphate from ungulate tooth enamel. *Quat. Res.* **75**, 605–613.

Feng X., Vico G. and Porporato A. (2012) On the effects of seasonality on soil water balance and plant growth: seasonality in water balance and plant growth. *Water Resour. Res.* **48**, 3.

Feranec R. S., Hadly E. A. and Paytan A. (2009) Stable isotopes reveal seasonal competition for resources between late Pleistocene bison (*Bison*) and horse (*Equus*) from Rancho La Brea, southern California. *Palaeogeogr. Palaeoclimatol. Palaeoecol.* **271**, 153–160.

Ferraro J. V., Plummer T. W., Pobiner B. L., Oliver J. S., Bishop L. C., Braun D. R., Ditchfield P., Binetti K. M., Seaman J. W., Hertel F. and Potts R. (2013) Earliest archaeological evidence of persistent hominin carnivory. *PLoS One* **8**, e62174.

Fick S. E. and Hijmans R. J. (2017) WorldClim 2: new 1-km spatial resolution climate surfaces for global land areas. *Int. J. Climatol.* **37**, 4302–4315.

Foley R. A. (1993) The influence of seasonality on hominid evolution. In *Seasonality and Human Ecology: 35th Symposium Volume of the Society for the Study of Human Biology* (eds. S. J. Ulijaszek and S. S. Strickland). Cambridge University Press, Cambridge, UK, pp. 17–37.

Fortelius M., Žliobaitė I., Kaya F., Bibi F., Bobe R., Leakey L., Leakey M., Patterson D., Rannikko J. and Werdelin L. (2016) An ecometric analysis of the fossil mammal record of the Turkana Basin. *Philos. Trans. R. Soc. Lond. B Biol. Sci.* **371**, 1–13.

Garcia N., Feranec R. S., Passey B. H., Cerling T. E. and Arsuaga J.-L. (2015) Exploring the potential of laser ablation carbon isotope analysis for examining ecology during the ontogeny of Middle Pleistocene Hominins from Sima de los Hueson (Northern Spain). *PLoS One* **10**, e0142895.

Good S. P. and Caylor K. K. (2011) Climatological determinants of woody cover in Africa. *Proc. Natl. Acad. Sci. U. S. A.* **108**, 4902–4907.

Green D. R., Green G. M., Colman A. S., Bidlack F. B., Tafforeau P. and Smith T. M. (2017) Synchrotron imaging and Markov Chain Monte Carlo reveal tooth mineralization patterns. *PLoS One* **12**, e0186391.

Green D. R., Smith T. M., Green G. M., Bidlack F. B., Tafforeau P. and Colman A. S. (2018b) Quantitative reconstruction of seasonality from stable isotopes in teeth. *Geochim. Cosmochim. Acta* **235**, 483–504.

Green D. R., Olack G. and Colman A. S. (2018a) Determinants of blood water $\delta^{18}O$ variation in a population of experimental sheep: implications for paleoclimate reconstruction. *Chem. Geol.* **485**, 32–43.

Guan K., Wolf A., Medvigy D., Caylor K. K., Pan M. and Wood E. F. (2013) Seasonal coupling of canopy structure and function in African tropical forests and its environmental controls. *Ecosphere* **4**, art35.

Guan K., Good S. P., Caylor K. K., Sato H., Wood E. F. and Li H. (2014) Continental-scale impacts of intra-seasonal rainfall variability on simulated ecosystem responses in Africa. *Biogeosciences* **11**, 6939–6954.

Guan K., Pan M., Li H., Wolf A., Wu J. and Medvigy D. (2015) Photosynthetic seasonality of global tropical forests constrained by hydroclimate. *Nat. Geosci.* **8**, 284–289.

Hailemichael M., Aronson J., Savin S., Tevesz M. J. S. and Carter J. G. (2002) $\delta^{18}O$ in mollusk shells from Pliocene Lake Hadar and modern Ethiopian lakes: implications for history of the Ethiopian monsoon. *Palaeogeogr. Palaeoclimatol. Palaeoecol.* **186**, 81–99.

Hartman G., Bar-Yosef O., Brittingham A., Grosman L. and Munro N. D. (2016) Hunted gazelles evidence cooling, but not drying, during the Younger Dryas in the southern Levant. *Proc. Natl. Acad. Sci. U. S. A.* **113**, 3997–4002.

Hay R. L. and Kyser T. K. (2001) Chemical sedimentology and paleoenvironmental history of Lake Olduvai, a Pliocene lake in northern Tanzania. *GSA Bulletin* **113**, 1505–1521.

Helliker B. R. and Ehleringer J. R. (2002) Differential ^{18}O enrichment of leaf cellulose in C_3 versus C_4 grasses. *Funct. Plant Biol.* **29**, 435–442.

Herbert T. D., Peterson L. C., Lawrence K. T. and Liu Z. (2010) Tropical ocean temperatures over the past 3.5 million years. *Science* **328**, 1530–1534.

Herrmann S. M. and Mohr K. I. (2011) A continental-scale classification of rainfall seasonality regimes in Africa based on gridded precipitation and land surface temperature products. *J. Appl. Meteorol. Climatol.* **50**, 2504–2513.

Hession S. L. and Moore N. (2011) A spatial regression analysis of the influence of topography on monthly rainfall in East Africa. *Int. J. Climatol.* **31**, 1440–1456.

Higgins P. and MacFadden B. J. (2004) "Amount Effect" recorded in oxygen isotopes of Late Glacial horse (*Equus*) and bison (*Bison*) teeth from the Sonoran and Chihuahuan deserts, southwestern United States. *Palaeogeogr. Palaeoclimatol. Palaeoecol.* **206**, 337–353.

Hiller C. R., Robinson C. and Weatherell J. A. (1975) Variations in the composition of developing rat incisor enamel. *Calcif. Tissue Res.* **18**, 1–12.

Hopley P. J., Weedon G. P., Brierley C. M., Thrasivoulou C., Herries A. I. R., Dinckal A., Richards D. A., Nita D. C., Parrish R. R., Roberts N. M. W., Sahy D. and Smith C. L. (2018) Orbital precession modulates interannual rainfall variability, as recorded in an Early Pleistocene speleothem. *Geology* **46**, 731–734.

Hoppe K. A. (2004) Late Pleistocene mammoth herd structure, migration patterns, and Clovis hunting strategies inferred from isotopic analyses of multiple death assemblages. *Paleobiology* **30**, 129–145.

Hoppe K. A., Stover S. M., Pascoe J. R. and Amundson R. (2004) Tooth enamel biomineralization in extant horses: implications for isotopic microsampling. *Palaeogeogr. Palaeoclimatol. Palaeoecol.* **206**, 355–365.

Hoppe K. A., Stuska S. and Amundson R. (2005) The implications for paleodietary and paleoclimatic reconstructions of intrapopulation variability in the oxygen and carbon isotopes of teeth from modern feral horses. *Quat. Res.* **64**, 138–146.

Huertas A. D., Iacumin P., Stenni B., Chillión B. S. and Longinelli A. (1995) Oxygen isotope variations of phosphate in mammalian bone and tooth enamel. *Geochim. Cosmochim. Acta* **59**, 4299–4305.

Iacumin P., Bocherens H. and Mariotti A. (1996) Oxygen isotope analyses of co-existing carbonate and phosphate in biogenic apatite: a way to monitor diagenetic alteration of bone phosphate? *Earth Planet. Sci. Lett.* **142**, 1–6.

Jacobs M. J. and Schloeder C. A. (2002) Fire frequency and species associations in perennial grasslands of south-west Ethiopia. *J. Ecol.* **40**, 1–9.

Jasechko S., Sharp Z. D., Gibson J. J., Birks S. J., Yi Y. and Fawcett P. J. (2013) Terrestrial water fluxes dominated by transpiration. *Nature* **496**, 347–350.

Johnson T. C., Scholz C. A., Talbot M. R., Kelts K., Ricketts R. D., Ngobi G., Beuning K., Ssemmanda I. I. and McGill J. W. (1996) Late Pleistocene desiccation of Lake Victoria and rapid evolution of cichlid fishes. *Science* **273**, 1091–1093.

Jones A. M., Iacumin P. and Young E. D. (1999) High-resolution $\delta^{18}O$ analysis of tooth enamel phosphate by isotope ratio monitoring gas chromatography mass spectrometry and ultraviolet laser fluorination. *Chem. Geol.* **153**, 241–248.

Joordens J. C. A., Vonhof H. B., Feibel C. S., Lourens L. J., Dupont-Nivet G., van der Lubbe J. H. J. L., Sier M. J., Davies G. R. and Kroon D. (2011) An astronomically-tuned climate framework for hominins in the Turkana Basin. *Earth Planet. Sci. Lett.* **307**, 1–8.

Julien M.-A., Rivals F., Serangeli J., Bocherens H. and Conard N. J. (2015) A new approach for deciphering between single and multiple accumulation events using intra-tooth isotopic variations: application to the Middle Pleistocene bone bed of Schöningen 13 II-4. *J. Hum. Evol.* **89**, 114–128.

Junginger A., Roller S., Olaka L. A. and Trauth M. H. (2014) The effects of solar irradiation changes on the migration of the Congo Air Boundary and water levels of paleo-Lake Suguta, Northern Kenya Rift, during the African Humid Period (15-5 ka BP). *Palaeogeogr. Palaeoclimatol. Palaeoecol.* **396**, 1–16.

Kaiser T. M., Seiffert C., Hertler C., Fiedler L., Fiedler L., Schwartz H. L., Frost S. R., Giemsch L., Bernor R. L., Wolf D., Semprebon G., Nelson S. V., Schrenk F., Harvati K., Bromage T. G. and Saanane C. (2010) Makuyuni, a new lower Palaeolithic hominid site in Tanzania. *Mitteilungen Hamburgisches Zoologisches Museum und Institut* **106**, 69–110.

Karp A. T., Behrensmeyer A. K. and Freeman K. H. (2018) Grassland fire ecology has roots in the late Miocene. *Proc. Natl. Acad. Sci. U. S. A.* **115**, 12130–12135.

Kent P. E. (1944) The Miocene beds of Kavirondo, Kenya. *Q. J. Geol. Soc. London* **100**, 85–118.

Kierdorf H., Kierdorf U., Frölich K. and Witzel C. (2013) Lines of Evidence-Incremental Markings in Molar Enamel of Soay Sheep as Revealed by a Fluorochrome Labeling and Backscattered Electron Imaging Study. *PLoS One* **8**, e74597.

Kimura Y., Jacobs L. L., Cerling T. E., Uno K. T., Ferguson K. M., Flynn L. J. and Patnaik R. (2013) Fossil mice and rats show isotopic evidence of niche partitioning and change in dental ecomorphology related to dietary shift in Late Miocene of Pakistan. *PLoS One* **8**, e69308.

King S. (2002) Home range and habitat use of free-ranging Przewalski horses at Hustai National Park Mongolia. *Appl. Anim. Behav. Sci.* **78**, 103–113.

Kingston J. D. (2005) Orbital controls on seasonality. In *Seasonality in Primates: Studies of Living and Extinct Humans and Non-Human Primates* (eds. D. K. Brockman and C. P. van Schaik). Cambridge University Press, Cambridge, UK, pp. 519–541.

Kingston J. D. (2007) Shifting adaptive landscapes: progress and challenges in reconstructing early hominid environments. *Am. J. Phys. Anthropol.*(Suppl 45), 20–58.

Kingston J. D., Deino A. L., Edgar R. and Hill A. (2007) Astronomically forced climate change in the Kenyan Rift Valley 2.7-2.55 Ma: implications for the evolution of early hominin ecosystems. *J. Hum. Evol.* **53**, 487–503.

Knapp A. K., Beier C., Briske D. D., Classen A. T., Luo Y., Reichstein M., Smith M. D., Smith S. D., Bell J. E., Fay P. A.,

Heisler, Leavitt S. W., Sherry R., Smith B. and Weng E. (2008) Consequences of more extreme precipitation regimes for terrestrial ecosystems. *Bioscience* **58**, 811–821.

Koch P. L., Tuross N. and Fogel M. L. (1997) The effects of sample treatment and diagenesis on the isotopic integrity of carbonate in biogenic hydroxylapatite. *J. Archaeol. Sci.* **24**, 417–429.

Kohn M. J. (1996) Predicting animal $\delta^{18}O$: Accounting for diet and physiological adaptation. *Geochim. Cosmochim. Acta* **60**, 4811–4829.

Kohn M. J. (2004) Comment: tooth enamel mineralization in ungulates: implications for recovering a primary isotopic time-series, by B. H. Passey and T. E. Cerling (2002). *Geochim. Cosmochim. Acta* **68**, 403–405.

Kohn M. J. and Cerling T. E. (2002) Stable isotope compositions of biological apatite. *Rev. Mineral. Geochem.*, 455–488.

Kohn M. J., Schoeninger M. J. and Valley J. W. (1996) Herbivore tooth oxygen isotope compositions: Effects of diet and physiology. *Geochim. Cosmochim. Acta* **60**, 3889–3896.

Kohn M. J., Schoeninger M. J. and Valley J. W. (1998) Variability in oxygen isotope compositions of herbivore teeth: reflections of seasonality or developmental physiology? *Chem. Geol.* **152**, 97–112.

Kohn M. J., Miselis J. L. and Fremd T. J. (2002) Oxygen isotope evidence for progressive uplift of the Cascade Range Oregon. *Earth Planet. Sci. Lett.* **204**, 151–165.

Konecky B. L., Noone D. C. and Cobb K. M. (2019) The influence of competing hydroclimate processes on stable isotope ratios in tropical rainfall. *Geophys. Res. Lett.* **22**, 449.

Lam Y. M. (2008) Variability in cementum deposition in springbok from the South African Cape. *J. Archaeol. Sci.* **35**, 1062–1073.

Larrasoaña J. C., Roberts A. P., Rohling E. J., Winklhofer M. and Wehausen R. (2003) Three million years of monsoon variability over the northern Sahara. *Clim. Dyn.* **21**, 689–698.

Lee-Thorp J. A. (2008) On isotopes and old bones. *Archaeometry* **50**, 925–950.

Lee-Thorp J., Likius A., Mackaye H. T., Vignaud P., Sponheimer M. and Brunet M. (2012) Isotopic evidence for an early shift to C_4 resources by Pliocene hominins in Chad. *Proc. Natl. Acad. Sci. U. S. A.* **109**, 20369–20372.

Lee-Thorp J. A. and Sponheimer M. (2003) Three case studies used to reassess the reliability of fossil bone and enamel isotope signals for paleodietary studies. *J. Anthropol. Archaeol.* **22**, 208–216.

Lee-Thorp J. A., Sponheimer M., Passey B. H., de Ruiter D. and Cerling T. E. (2010) Stable isotopes in fossil hominin tooth enamel suggest a fundamental dietary shift in the Pliocene. *Phil. Trans. R. Soc. B* **365**, 3389–3396.

LeGeros R. Z., Trautz O. R., Klein E. and LeGeros J. P. (1969) Two types of carbonate substitution in the apatite structure. *Experientia* **25**, 5–7.

Lehmann C. E. R., Anderson T. M., Sankaran M., Higgins S. I., Archibald S., Hoffmann W. A., Hanan N. P., Williams R. J., Fensham R. J., Felfili J., Hutley L. B., Ratnam J., José J. S., Montes R., Franklin D., Russell-Smith J., Ryan C. M., Durigan G., Hiernaux P., Haidar R., Bowman D. M. J. S. and Bond W. J. (2014) Savanna vegetation-fire-climate relationships differ among continents. *Science* **343**, 548–552.

Lehmann S. B., Levin N. E., Braun D. R., Stynder D. D., Zhu M., le Roux P. J. and Sealy J. (2018) Environmental and ecological implications of strontium isotope ratios in mid-Pleistocene fossil teeth from Elandsfontein, South Africa. *Palaeogeogr. Palaeoclimatol. Palaeoecol.* **490**, 84–94.

Lemorini C., Plummer T. W., Braun D. R., Crittenden A. N., Ditchfield P., Bishop L. C., Hertel F., Oliver J. S., Marlowe F. W., Schoeninger M. J. and Potts R. (2014) Old stones' song: Use-wear experiments and analysis of the Oldowan quartz and quartzite assemblage from Kanjera South (Kenya). *J. Hum. Evol.* **72**, 10–25.

Lepre C. J., Quinn R. L., Joordens J. C. A., Swisher C. C. III. and Feibel C. S. (2007) Plio-Pleistocene facies environments from the KBS Member, Koobi Fora Formation: implications for climate controls on the development of lake-margin hominin habitats in the northeast Turkana Basin (northwest Kenya). *J. Hum. Evol.* **53**, 504–514.

Levin N. E. (2015) Environment and climate of early human evolution. *Annu. Rev. Earth Planet. Sci.* **43**, 405–429.

Levin N. E., Cerling T. E., Passey B. H., Harris J. M. and Ehleringer J. R. (2006) A stable isotope aridity index for terrestrial environments. *Proc. Natl. Acad. Sci. U. S. A.* **103**, 11201–11205.

Levin N. E., Zipser E. J. and Cerling T. E. (2009) Isotopic composition of waters from Ethiopia and Kenya: insights into moisture sources for eastern Africa. *J. Geophys. Res.* **114**, D23306.

Levin N. E., Brown F. H., Behrensmeyer A. K., Bobe R. and Cerling T. E. (2011) Paleosol carbonates from the Omo Group: isotopic records of local and regional environmental change in East Africa. *Palaeogeogr. Palaeoclimatol. Palaeoecol.* **307**, 75–89.

Liddy H. M., Feakins S. J. and Tierney J. E. (2016) Cooling and drying in northeast Africa across the Pliocene. *Earth Planet. Sci. Lett.* **449**, 430–438.

Liutkus C. M., Wright J. D., Ashley G. M. and Sikes N. E. (2005) Paleoenvironmental interpretation of lake-margin deposits using $\delta^{13}C$ and $\delta^{18}O$ results from early Pleistocene carbonate rhizoliths, Olduvai Gorge, Tanzania. *Geology* **33**, 377–380.

Lüdecke T., Mulch A., Kullmer O., Sandrock O., Thiemeyer H., Fiebig J. and Schrenk F. (2016) Stable isotope dietary reconstructions of herbivore enamel reveal heterogeneous savanna ecosystems in the Plio-Pleistocene Malawi Rift. *Palaeogeogr. Palaeoclimatol. Palaeoecol.* **459**, 170–181.

Lupien R. L., Russell J. M., Feibel C., Beck C., Castañeda I., Deino A. and Cohen A. S. (2018) A leaf wax biomarker record of early Pleistocene hydroclimate from West Turkana Kenya. *Quat. Sci. Rev.* **186**, 225–235.

MacFadden B. J. (2008) Geographic variation in diets of ancient populations of 5-million-year-old (early Pliocene) horses from southern North America. *Palaeogeogr. Palaeoclimatol. Palaeoecol.* **266**, 83–94.

Macho G. A., Reid D., Leakey M. G., Jablonski N. G. and Beynon A. D. (1996) Climatic effects on dental development of Theropithecus oswaldi from Koobi Fora and Olorgesailie. *J. Hum. Evol.* **30**, 57–70.

Macho G. A., Leakey M. G., Williamson D. K. and Jiang Y. (2003) Palaeoenvironmental reconstruction: evidence for seasonality at Allia Bay, Kenya, at 3.9 million years. *Palaeogeogr. Palaeoclimatol. Palaeoecol.* **199**, 17–30.

Macho G. A. and Leakey M. G. (2009) Small-scale environmental fluctuations and their possible effects on cognitive evolution and migration of Homo. *Quat. Int.* **204**, 95–97.

Makarewicz C. A. and Pederzani S. (2017) Oxygen ($\delta^{18}O$) and carbon ($\delta^{13}C$) isotopic distinction in sequentially sampled tooth enamel of co-localized wild and domesticated caprines: complications to establishing seasonality and mobility in herbivores. *Palaeogeogr. Palaeoclimatol. Palaeoecol.* **485**, 1–15.

Martin C., Bentaleb I., Kaandorp R., Iacumin P. and Chatri K. (2008) Intra-tooth study of modern rhinoceros enamel $\delta^{18}O$: Is the difference between phosphate and carbonate $\delta^{18}O$ a sound diagenetic test? *Palaeogeogr. Palaeoclimatol. Palaeoecol.* **266**, 183–189.

Maslin M. A., Brierley C. M., Milner A. M., Shultz S., Trauth M. H. and Wilson K. E. (2014) East African climate pulses and early human evolution. *Quat. Sci. Rev.* **101**, 1–17.

McHenry L. J. and de la Torre I. (2018) Hominin raw material procurement in the Oldowan-Acheulean transition at Olduvai Gorge. *J. Hum. Evol.* **120**, 378–401.

McHenry L. J. and Stanistreet I. G. (2018) Tephrochronology of Bed II, Olduvai Gorge, Tanzania, and placement of the Oldowan-Acheulean transition. *J. Hum. Evol.* **120**, 7–18.

Merlis T. M., Schneider T., Bordoni S. and Eisenman I. (2013) The tropical precipitation response to orbital precession. *J. Clim.* **26**, 2010–2021.

Metcalfe J. Z. and Longstaffe F. J. (2012) Mammoth tooth enamel growth rates inferred from stable isotope analysis and histology. *Quat. Res.* **77**, 424–432.

Metcalfe J. Z. and Longstaffe F. J. (2014) Environmental change and seasonal behavior of mastodons in the Great Lakes region inferred from stable isotope analysis. *Quat. Res.* **82**, 366–377.

Meyer A., Kocher T. D., Basasibwaki P. and Wilson A. C. (1990) Monophyletic origin of Lake Victoria cichlid fishes suggested by mitochondrial DNA sequences. *Nature* **347**, 550–553.

Moss-Salentijn L., Moss M. L. and Yuan M. S.-T. (1997) The ontogeny of mammalian enamel. In *Tooth Enamel Microstructure*. Balkema, Rotterdam, pp. 5–30.

Nacarino-Meneses C., Jordana X., Orlandi-Oliveras G. and Köhler M. (2017) Reconstructing molar growth from enamel histology in extant and extinct Equus. *Sci. Rep.* **7**, 15965.

Nelson S. V. (2005) Paleoseasonality inferred from equid teeth and intra-tooth isotopic variability. *Palaeogeogr. Palaeoclimatol. Palaeoecol.* **222**, 122–144.

Nicholson S. E. (1996) A review of climate dynamics and climate variability in Eastern Africa. In *The Limnology, Climatology, and Paleoclimatology of the East African Lakes* (eds. E. O. O. Thomas and C. Johnson). Gordon and Breach, Amsterdam, pp. 25–56.

Nicholson S. E. (2000) The nature of rainfall variability over Africa on time scales of decades to millenia. *Glob. Planet. Change* **26**, 137–158.

Nicholson S. (2016) The Turkana low-level jet: mean climatology and association with regional aridity. *Int. J. Climatol.* **36**, 2598–2614.

Nicholson S. E. (2017) Climate and climatic variability of rainfall over eastern Africa. *Rev. Geophys.* **55**, 590–635.

Nicholson S. E. (2018) The ITCZ and the Seasonal Cycle over Equatorial Africa. *Bull. Am. Meteorol. Soc.* **99**, 337–348.

Oettli P. and Camberlin P. (2005) Influence of topography on monthly rainfall distribution over East Africa. *Clim. Res.* **28**, 199–212.

Ogallo L. J. (1989) The spatial and temporal patterns of the East African seasonal rainfall derived from principal component analysis. *Int. J. Climatol.* **9**, 145–167.

Ogutu J. O. and Owen-Smith N. (2003) ENSO, rainfall and temperature influences on extreme population declines among African savanna ungulates. *Ecol. Lett.* **6**, 412–419.

Ogutu J. O., Piepho H. P., Reid R. S. and Rainy M. E. (2010) Large herbivore responses to water and settlements in savannas. *Ecol. Monogr.* **80**, 241–266.

Osborne C. P. (2008) Atmosphere, ecology and evolution: what drove the Miocene expansion of C_4 grasslands? *J. Ecol.* **96**, 35–45.

Pante M. C., Njau J. K., Hensley-Marschand B., Keevil T. L., Martín-Ramos C., Peters R. F. and de la Torre I. (2018) The carnivorous feeding behavior of early *Homo* at HWK EE, Bed II, Olduvai Gorge Tanzania. *J. Hum. Evol.* **120**, 215–235.

Passey B. H. and Cerling T. E. (2002) Tooth enamel mineralization in ungulates: implications for recovering a primary isotopic time-series. *Geochim. Cosmochim. Acta* **66**, 3225–3234.

Passey B. H. and Cerling T. E. (2004) Response to the comment by M. J. Kohn on "Tooth Enamel Mineralization in Ungulates: Implications for Recovering a Primary Isotopic Time-Series", by B. H. Passey and T. E. Cerling (2002). *Geochim. Cosmochim. Acta* **68**, 407–409.

Passey B. H., Cerling T. E., Schuster G. T., Robinson T. F., Roeder B. L. and Krueger S. K. (2005) Inverse methods for estimating primary input signals from time-averaged isotope profiles. *Geochim. Cosmochim. Acta* **69**, 4101–4116.

Passey B. H. and Cerling T. E. (2006) In situ stable isotope analysis ($\delta^{13}C$, $\delta^{18}O$) of very small teeth using laser ablation GC/IRMS. *Chem. Geol.* **235**, 238–249.

Pellegrini M., Donahue R. E., Chenery C., Evans J., Lee-Thorp J. A., Montgomery J. and Mussi M. (2008) Faunal migration in late-glacial central Italy: implications for human resource exploitation. *Rapid Commun. Mass Spectrom.* **22**, 1714–1726.

Pellegrini M., Lee-Thorp J. A. and Donahue R. E. (2011) Exploring the variation of the $\delta^{18}O_p$ and $\delta^{18}O_c$ relationship in enamel increments. *Palaeogeogr. Palaeoclimatol. Palaeoecol.* **310**, 71–83.

Peppe D. J., Royer D. L., Cariglino B., Oliver S. Y., Newman S., Leight E., Enikolopov G., Fernandez-Burgos M., Herrera F., Adams J. M., Correa E., Currano E. D., Erickson J. M., Hinojosa L. F., Hoganson J. W., Iglesias A., Jaramillo C. A., Johnson K. R., Jordan G. J., Kraft N. J. B., Lovelock E. C., Lusk C. H., Niinemets U., Peñuelas J., Rapson G., Wing S. L. and Wright I. J. (2011) Sensitivity of leaf size and shape to climate: global patterns and paleoclimatic applications. *New Phytol.* **190**, 724–739.

Plummer T. W. (1991) *Site formation and paleoecology at the Early to Middle Pleistocene locality of Kanjera, Kenya* Ph.D. Dissertation. Yale University.

Plummer T. and Bishop L. (2016) Oldowan hominin behavior and ecology at Kanjera South Kenya. *J. Anthropol. Sci.* **94**, 29–40.

Plummer T. W., Ditchfield P. W., Bishop L. C., Kingston J. D., Ferraro J. V., Braun D. R., Hertel F. and Potts R. (2009b) Oldest evidence of tool making hominins in a grassland-dominated ecosystem. *PLoS One* **4**, e7199.

Plummer T. W., Bishop L. C., Ditchfield P. W., Ferraro J. V., Kingston J. D., Hertel F. and Braun D. R. (2009a) The environmental context of oldowan hominin activities at Kanjera South, Kenya. In *Interdisciplinary Approaches to the Oldowan Vertebrate Paleobiology and Paleoanthropology* (eds. E. Hovers and D. R. Braun). Springer, Dordrecht, pp. 149–160.

Podlesak D. W., Torregrossa A. M., Ehleringer J. R., Dearing M. D., Passey B. H. and Cerling T. E. (2008) Turnover of oxygen and hydrogen isotopes in the body water, CO_2, hair, and enamel of a small mammal. *Geochim. Cosmochim. Acta* **72**, 19–35.

Potts R. (2013) Hominin evolution in settings of strong environmental variability. *Quat. Sci. Rev.* **73**, 1–13.

Potts R. and Faith J. T. (2015) Alternating high and low climate variability: The context of natural selection and speciation in Plio-Pleistocene hominin evolution. *J. Hum. Evol.* **87**, 5–20.

Reade H., O'Connell T. C., Barker G. and Stevens R. E. (2018) Increased climate seasonality during the late glacial in the Gebel Akhdar Libya. *Quat. Sci. Rev.* **192**, 225–235.

Redfern J. V., Grant R., Biggs H. and Getz W. M. (2003) Surface-water constraints on herbivore foraging in the Kruger National Park, South Africa. *Ecology* **84**, 2092–2107.

Retallack G. J. (2005) Pedogenic carbonate proxies for amount and seasonality of precipitation in paleosols. *Geology* **33**, 333–336.

Risi C., Bony S. and Vimeux F. (2008) Influence of convective processes on the isotopic composition ($\delta^{18}O$ and δD) of precipitation and water vapor in the tropics: 2. Physical interpretation of the amount effect. *J. Geophys. Res.* **113**, 3158.

Rivals F., Julien M.-A., Kuitems M., van Kolfschoten T., Serangeli J., Drucker D. G., Bocherens H. and Conard N. J. (2014) Investigation of equid paleodiet from Schöningen 13 II-4 through dental wear and isotopic analyses: Archaeological implications. *J. Hum. Evol.* **89**, 129–137.

Robinson C., Fuchs P., Deutsch D. and Weatherell J. A. (1978) Four chemically distinct stages in developing enamel from bovine incisor teeth. *Caries Res.* **12**, 1–11.

Robinson C., Briggs H. D., Atkinson P. J. and Weatherell J. A. (1979) Matrix and mineral changes in developing enamel. *J. Dent. Res.* **58**, 871–882.

Robinson C., Kirkham J., Brookes S. J., Bonass W. A. and Shore R. C. (1995) The chemistry of enamel development. *Int. J. Dev. Biol.* **39**, 145–152.

Robinson C., Brookes S. J., Bonass W. A., Shore R. C. and Kirkham J. (1997) Enamel maturation. In *Dental Enamel* (eds. D. Chadwick and G. Cardew). Wiley Online Library, Chichester, UK, pp. 156–174.

Roche D., Ségalen L., Balan E., Balan E. and Delattre S. (2010) Preservation assessment of Miocene-Pliocene tooth enamel from Tugen Hills (Kenyan Rift Valley) through FTIR, chemical and stable-isotope analyses. *J. Archaeol. Sci.* **37**, 1690–1699.

Rohr T., Manzoni S., Feng X., Menezes R. S. C. and Porporato A. (2013) Effect of rainfall seasonality on carbon storage in tropical dry ecosystems. *J. Geophys. Res.: Biogeosci.* **118**, 1156–1167.

Rose C., Polissar P. J., Tierney J. E., Filley T. and deMenocal P. B. (2016) Changes in northeast African hydrology and vegetation associated with Pliocene-Pleistocene sapropel cycles. *Philos. Trans. R. Soc. Lond. B Biol. Sci.* **371**, 20150243.

Rossignol-Strick M. (1983) African monsoons, an immediate climate response to orbital insolation. *Nature* **304**, 46–49.

Rozanski K., Araguas-Araguas L. and Gonfiantini R. (1993) Isotopic patterns in modern global precipitation. In *Climate Change in Continental Isotopic Records* (eds. S. Pk, L. Kc, M. J and S. S). American Geophysical Union, pp. 1–36.

Rozanski K., Araguas-Araguas L. and Gonfiantini R. (1996) Isotope patterns of precipitation in the East African region. In *The Limnology, Climatology, and Paleoclimatology of the East African lakes* (eds. T. C. Johnson and E. O. Odada). Gordon and Breach, Amsterdam, pp. 79–93.

Runyan C. W. and D'Odorico P. (2013) Positive feedbacks and bistability associated with phosphorus–vegetation–microbial interactions. *Adv. Water Resour.* **52**, 151–164.

Sánchez-Hernández C., Rivals F., Blasco R. and Rosell J. (2016) Tale of two timescales: Combining tooth wear methods with different temporal resolutions to detect seasonality of Palaeolithic hominin occupational patterns. *J. Archaeol. Sci.: Rep.* **6**, 790–797.

Scheibe K. M., Eichhorn K., Kalz B., Streich W. J. and Scheibe A. (1998) Water consumption and watering behavior of Przewalski horses (Equus ferus przewalskii) in a semireserve. *Zool. Biol.* **17**, 191–192.

Schwartz H., Renne P. R., Morgan L. E., Wildgoose M. M., Lippert P. C., Frost S. R., Harvati K., Schrenk F. and Saanane C. (2012) Geochronology of the Manyara Beds, northern Tanzania: new tephrostratigraphy, magnetostratigraphy and $^{40}Ar/^{39}Ar$ ages. *Quat. Geochronol.* **7**, 48–66.

Sharp Z. D. and Cerling T. E. (1998) Fossil isotope records of seasonal climate and ecology: straight from the horse's mouth. *Geology* **26**, 219–222.

Sikes N. E. (1994) Early hominid habitat preferences in East Africa: paleosol carbon isotopic evidence. *J. Hum. Evol.* **27**, 25–45.

Sikes N. E. and Ashley G. M. (2007) Stable isotopes of pedogenic carbonates as indicators of paleoecology in the Plio-Pleistocene (upper Bed I), western margin of the Olduvai Basin, Tanzania. *J. Hum. Evol.* **53**, 574–594.

Simmer J. P., Richardson A. S., Hu Y. Y., Smith C. E. and Hu J. C.-C. (2012) A post-classical theory of enamel biomineralization... and why we need one. *Int. J. Oral Sci.* **4**, 129–134.

Sitters J., Heitkönig I. M. A., Holmgren M. and Ojwang' G. S. O. (2009) Herded cattle and wild grazers partition water but share forage resources during dry years in East African savannas. *Biol. Conserv.* **142**, 738–750.

Smith C. E. (1998) Cellular and chemical events during enamel maturation. *Crit. Rev. Oral Biol. Med.* **9**, 128–161.

Souron A., Balasse M. and Boisserie J.-R. (2012) Intra-tooth isotopic profiles of canines from extant *Hippopotamus amphibius* and late Pliocene hippopotamids (Shungura Formation, Ethiopia): Insights into the seasonality of diet and climate. *Palaeogeogr. Palaeoclimatol. Palaeoecol.* **342**, 97–110.

Sponheimer M. and Cerling T. E. (2014) Investigating ancient diets using stable isotopes in bioapatites. In *Treatise on Geochemistry Volume 14: Archaeology and Anthropology* (ed. T. E. Cerling). Elsevier, pp. 341–355.

Sponheimer M., Passey B. H., de Ruiter D. J., Guatelli-Steinberg D., Cerling T. E. and Lee-Thorp J. A. (2006) Isotopic evidence for dietary variability in the early hominin *Paranthropus robustus*. *Science* **314**, 980–982.

Stacy E. (2008) *Stable Isotopic Analysis of Equid (Horse) Teeth from Mongolia* Unpublished Thesis. University of Pittsburgh.

Stager J. C., Cumming B. F. and Meeker L. D. (2003) A 10,000-year high-resolution diatom record from Pilkington Bay, Lake Victoria, East Africa. *Quat. Res.* **59**, 172–181.

Stanistreet I. G., McHenry L. J., Stollhofen H. and de la Torre I. (2018) Bed II sequence stratigraphic context of EF-HR and HWK EE archaeological sites, and the Oldowan/Acheulean succession at Olduvai Gorge, Tanzania. *J. Hum. Evol.* **120**, 19–31.

Staver A. C., Archibald S. and Levin S. A. (2011) The global extent and determinants of savanna and forest as alternative biome states. *Science* **334**, 230–232.

Strömberg C. A. E. (2011) Evolution of grasses and grassland ecosystems. *Annu. Rev. Earth Planet. Sci.* **39**, 517–544.

Suga S. (1982) Progressive mineralization pattern of developing enamel during the maturation stage. *J. Dent. Res.*, 1532–1542.

Suga S. (1983) Comparative histology of the progressive mineralization pattern of developing enamel. In *Mechanisms of Tooth Enamel Formation* (ed. S. Suga). Quintessence Publishing, Tokyo, pp. 167–203.

Sun X., Xie L., Semazzi F. and Liu B. (2015) Effect of Lake Surface Temperature on the Spatial Distribution and Intensity of the Precipitation over the Lake Victoria Basin. *Mon. Weather Rev.* **143**, 1179–1192.

Sydney-Zax M., Mayer I. and Deutsch D. (1991) Carbonate content in developing human and bovine enamel. *J. Dent. Res.* **70**, 913–916.

Tafforeau P., Bentaleb I., Jaeger J. J. and Martin C. (2007) Nature of laminations and mineralization in rhinoceros enamel using histology and X-ray synchrotron microtomography: potential implications for palaeoenvironmental isotopic studies. *Palaeogeogr. Palaeoclimatol. Palaeoecol.* **246**, 206–227.

Tappen M. (1994) Bone weathering in the tropical rain forest. *J. Archaeol. Sci.* **21**, 667–673.

Terzer S., Wassenaar L. I., Araguás-Araguás L. J. and Aggarwal P. K. (2013) Global isoscapes for $\delta^{18}O$ and $\delta^{2}H$ in precipitation:

improved prediction using regionalized climatic regression models. *Hydrol. Earth Syst. Sci.* **17**, 4713–4728.
Thornthwaite C. W. (1948) An approach toward a rational classification of climate. *Geogr. Rev.* **38**, 55–94.
Tiedemann R., Sarnthein M. and Shackleton N. J. (1994) Astronomic timescale for the Pliocene Atlantic $\delta^{18}O$ and dust flux records of ocean drilling program site 659. *Paleoceanography* **9**, 619–638.
Trauth M. H., Maslin M. A., Deino A. L. and Strecker M. R. (2005) Late Cenozoic Moisture History of East Africa. *Science* **309**, 2051–2053.
Trauth M. H., Maslin M. A., Deino A. L., Strecker M. R., Bergner A. G. N. and Dühnforth M. (2007) High- and low-latitude forcing of Plio-Pleistocene East African climate and human evolution. *J. Hum. Evol.* **53**, 475–486.
Trauth M. H., Larrasoaña J. C. and Mudelsee M. (2009) Trends, rhythms and events in Plio-Pleistocene African climate. *Quat. Sci. Rev.* **28**, 399–411.
Trayler R. B. and Kohn M. J. (2017) Tooth enamel maturation reequilibrates oxygen isotope compositions and supports simple sampling methods. *Geochim. Cosmochim. Acta* **198**, 32–47.
Uno K. T., Cerling T. E., Harris J. M., Kunimatsu Y., Leakey M. G., Nakatsukasa M. and Nakaya H. (2011) Late Miocene to Pliocene carbon isotope record of differential diet change among East African herbivores. *Proc. Natl. Acad. Sci. U. S. A.* **108**, 6509–6514.
Uno K. T., Rivals F., Bibi F., Pante M., Njau J. and de la Torre I. (2018) Large mammal diets and paleoecology across the Oldowan-Acheulean transition at Olduvai Gorge Tanzania from stable isotope and tooth wear analyses. *J. Hum. Evol.* **120**, 76–91.
van Dam J. A. and Reichart G. J. (200) Oxygen and carbon isotope signatures in late Neogene horse teeth from Spain and application as temperature and seasonality proxies. *Palaeogeogr. Palaeoclimatol. Palaeoecol.* **274**, 64–81.
Verschuren D., Sinninghe Damsté J. S., Moernaut J., Kristen I., Blaauw M., Fagot M., Haug G. H. and CHALLACEA Project Members (2009) Half-precessional dynamics of monsoon rainfall near the East African Equator. *Nature* **462**, 637–641.
Vincens A., Garcin Y. and Buchet G. (2007) Influence of rainfall seasonality on African lowland vegetation during the Late Quaternary: pollen evidence from Lake Masoko, Tanzania. *J. Biogeogr.* **34**, 1274–1288.
Viste E. and Sorteberg A. (2013) Moisture transport into the Ethiopian highlands. *Int. J. Climatol.* **33**, 249–263.
Vonhof H. B., Joordens J. C. A., Noback M. L., van der Lubbe J. H. J. L., Feibel C. S. and Kroon D. (2013) Environmental and climatic control on seasonal stable isotope variation of freshwater molluscan bivalves in the Turkana Basin (Kenya). *Palaeogeogr. Palaeoclimatol. Palaeoecol.* **383**, 16–26.
Wallace J. P., Crowley B. E. and Miller J. H. (2019) Investigating equid mobility in Miocene Florida, USA using strontium isotope ratios. *Palaeogeogr. Palaeoclimatol. Palaeoecol.* **516**, 232–243.
Wall-Scheffler C. M. and Foley R. A. (2008) Digital cementum luminance analysis (DCLA): a tool for the analysis of climatic and seasonal signals in dental cementum. *Int. J. Osteoarchaeol.* **18**, 11–27.
Wang Y. and Cerling T. E. (1994) A model of fossil tooth and bone diagenesis: implications for paleodiet reconstruction from stable isotopes. *Palaeogeogr. Palaeoclimatol. Palaeoecol.* **107**, 281–289.
Wang Y., Kromhout E., Zhang C., Xu Y., Parker W., Deng T. and Qiu Z. (2008) Stable isotopic variations in modern herbivore tooth enamel, plants and water on the Tibetan Plateau: Implications for paleoclimate and paleoelevation reconstructions. *Palaeogeogr. Palaeoclimatol. Palaeoecol.* **260**, 359–374.
Wara M. W., Ravelo A. C. and Delaney M. L. (2005) Permanent El Niño-like conditions during the Pliocene warm period. *Science* **309**, 758–761.
Weatherell J. A., Robinson C. and Hiller C. R. (1968) Distribution of carbonate in thin sections of dental enamel. *Caries Res.* **2**, 1–9.
Western D. (1975) Water availability and its influence on the structure and dynamics of a savannah large mammal community. *Afr. J. Ecol.* **13**, 265–286.
Wiedemann F. B., Bocherens H., Mariotti A., Driesch A. von. D. and Grupe G. (1999) Methodological and Archaeological Implications of Intra-tooth Isotopic Variations ($\delta^{13}C$, $\delta^{18}O$) in Herbivores from Ain Ghazal (Jordan, Neolithic). *J. Archaeol. Sci.* **26**, 697–704.
Wilson K. E., Maslin M. A., Leng M. J., Kingston J. D., Deino A. L., Edgar R. K. and Mackay A. W. (2014) East African lake evidence for Pliocene millennial-scale climate variability. *Geology* **42**, 955–958.
Wolf D., Nelson S. V., Schwartz H. L., Semprebon G. M., Kaiser T. M. and Bernor R. L. (2010) Taxonomy and paleoecology of the Pleistocene Equidae from Makuyuni, northern Tanzania. *Palaeodiversity* **3**, 249–269.
Yang W., Seager R., Cane M. A. and Lyon B. (2015) The annual cycle of east African precipitation. *J. Clim.* **28**, 2385–2404.
Yin X., Nicholson S. E. and Ba M. B. (2000) On the diurnal cycle of cloudiness over Lake Victoria and its influence on evaporation from the lake. *Hydrol. Sci. J.* **45**, 407–424.
Zanazzi A., Judd E., Fletcher A., Bryant H. and Kohn M. J. (2015) Eocene-Oligocene latitudinal climate gradients in North America inferred from stable isotope ratios in perissodactyl tooth enamel. *Palaeogeogr. Palaeoclimatol. Palaeoecol.* **417**, 561–568.
Zazzo A., Lécuyer C. and Mariotti A. (2004) Experimentally-controlled carbon and oxygen isotope exchange between bioapatites and water under inorganic and microbially-mediated conditions. *Geochim. Cosmochim. Acta* **68**, 1–12.
Zazzo A., Balasse M. and Patterson W. P. (2005) High-resolution $\delta^{13}C$ intratooth profiles in bovine enamel: implications for mineralization pattern and isotopic attenuation. *Geochim. Cosmochim. Acta* **69**, 3631–3642.
Zazzo A., Balasse M. and Patterson W. P. (2006) The reconstruction of mammal individual history: refining high-resolution isotope record in bovine tooth dentine. *J. Archaeol. Sci.* **33**, 1177–1187.
Zazzo A., Balasse M., Passey B. H., Moloney A. P., Monahan F. J. and Schmidt O. (2010) The isotope record of short- and long-term dietary changes in sheep tooth enamel: implications for quantitative reconstruction of paleodiets. *Geochim. Cosmochim. Acta* **74**, 3571–3586.
Zazzo A., Bendrey R., Vella D., Moloney A. P., Monahan F. J. and Schmidt O. (2012) A refined sampling strategy for intra-tooth stable isotope analysis of mammalian enamel. *Geochim. Cosmochim. Acta* **84**, 1–13.
Zhang C., Wang Y., Deng T., Wang X., Biasatti D., Xu Y. and Li Q. (2009) C4 expansion in the central Inner Mongolia during the latest Miocene and early Pliocene. *Earth Planet. Sci. Lett.* **287**, 311–319.
Zhang C., Wang Y., Li Q., Wang X. and Deng T. (2012) Diets and environments of late Cenozoic mammals in the Qaidam Basin, Tibetan Plateau: Evidence from stable isotopes. *Earth Planet. Sci. Lett.* **333–334**, 70–82.

Associate editor: Miryam Bar-Matthews